LHCb-ANA-2010-015
June 16, 2011

Measurement of b-hadron production fractions in 7 TeV centre-of-mass energy pp collisions

M. Artuso, A. Borgia, S. Stone, P. Uriquijo, Z. Xing, L. Zhang

Syracuse University, Syracuse NY 13244, USA

Abstract

This note describes the determination of b-quark fragmentation into bottom hadrons in proton-proton collisions at a centre-of-mass energy of 7 TeV. The analysis uses semileptonic decays of the b-flavoured hadrons, identified by the detection of a muon and a charmed hadron. We study the dependence of the ratios of strange B mesons to light B mesons $[f_s/(f_u+f_d)]$ and Λ_b baryons to light B mesons $[f_{\Lambda_b}/(f_u+f_d)]$ as a function of the transverse momentum of the charmed hadron-muon system (p_t). We find that $[f_s/(f_u+f_d)]$ is independent of the transverse momentum of the $D_s\mu$ pair and of the pseudo-rapidity η of the b-hadron, and we determine $[f_s/(f_u+f_d)]$ as $0.134\pm0.004^{+0.011}_{-0.010}$, where the first error is statistical and the second systematic. The corresponding ratio $[f_{\Lambda_b}/(f_u+f_d)]$ is found to be dependent upon the transverse momentum of the $\Lambda_c\mu$ pair, but independent of η. Thus we quote $[f_{\Lambda_b}/(f_u+f_d)] = (0.404\pm0.017(stat)\pm0.027(sys)\pm0.105(Br))\times[1-(0.031\pm0.004\pm0.003)\times p_t(\mathrm{GeV})]$, where the errors on the scale are statistical, systematic, and the last error reflects an absolute scale uncertainty due to the poorly known $\mathcal{B}(\Lambda_c\to pK\pi)$. Our investigation of $\overline{B}{}^0_s$ decays into $D^0K^+X\mu^-\overline{\nu}$ final states reveals the first observation of $\overline{B}{}^0_s \to D^{*+}_{s2}X\mu^-\overline{\nu}$ decays. A study of the b-hadron production cross section as a function of p_t and η will be the object of a future paper.

Contents

Table 1: Charm hadron decay modes and branching fractions

Particle	Final State	Branching Fraction (%)
D^0	$K^-\pi^+$	3.89±0.05 [1]
D^+	$K^-\pi^+\pi^+$	9.14±0.20 [2]
D_s	$K^-K^+\pi^+$	5.50±0.27 [3]
Λ_c	$pK^-\pi^+$	5.0±1.3 [1]

1 Introduction

Knowledge of the production rates of b-flavoured hadrons in proton-proton collisions at the LHC is essential to extract measurements of absolute branching fractions from the data. Since absolute branching fractions of many decays of B^- and $\overline{B}^0$ have been well measured at e^+e^- colliders [1], it suffices to measure the ratio of B_s or Λ_b production to either B^- or $\overline{B}^0$ production. The relative fractions, however, are not well predicted by models, and thus must be measured. In what follows we will assume isospin symmetry so that the yields of B^- and $\overline{B}^0$ are taken as equal, and we will average the yields of b and $\overline{b}$ final states, so that the mention of a specific final state will refer also to its charge-conjugate. Much of the analysis method is adapted from the study of the η dependence of the production cross-section in the region $2 < \eta < 6$ than we previously published [4]. Here $\eta = -\ln(\tan(\theta/2))$, and θ is the angle of the b-flavored hadron with respect to the proton direction. In this note we focus on the region $2 \le \eta \le 5$. *We assume that readers of this note are familiar with the material in [4].*

The data sample for this analysis uses triggers designed to select a single muon in the first 3 pb^{-1} of data taking. The maximum average number of interactions per crossing reached 1.5 at the beginning of the run. The TCK's that were used include 0x12001F 0x10001F 0x14001F 0x13001F 0x18001F 0x17001F 0x19001F 0x1A001F 0x190023 0x190024. For higher level triggers we use Hlt1SingleMuonNoIP and Hlt2SingleMuon. We measure the HLT1 and HLT2 single muon efficiencies using TIS J/ψ from the lifetime biased dimuon stripping line.

We use Rec05Stripping09 processed using DaVinci v25r7(8) and Brunel v37r6p1. Monte Carlo simulation uses Pythia 6.4 [5]. We generated 400-1500K events per channel using Gauss v38r8, Boole v21r7, and Brunel v37r6p1.

We select events containing a charmed hadron that forms a common vertex with the trigger muon. The charm hadrons and their branching fractions to the states that we detect are listed in Table 1. Each of these different charm hadron plus muon final states can be populated by a mixture of initial b hadron states. $\overline{B}^0$ mesons decay semileptonically into a mixture of D^0 and D^+ mesons, while B^- mesons decay predominantly into D^0 mesons with a smaller admixture of D^+ mesons. $\overline{B}_s^0$ mesons decay predominantly into D_s^+ mesons, but can also decay into D^0K^+ and D^+K_s mesons; this is expected if the B_s decays into a D_s^{**} state that is heavy enough to decay into a DK pair. In this note we will measure this contribution using $D^0K^+X\mu^-\overline{\nu}$ events. Thus the $\overline{B}_s^0$ semileptonic yield is largely due to $D_s^+X\mu^-\overline{\nu}$ events, but includes $\overline{B}_s^0 \to DK\mu^-\overline{\nu}X$ decays, and needs to be corrected for a small component of $D_s\mu^-\overline{\nu}X$ events originating from $B^-(\overline{B}^0) \to D_sK\mu^-\overline{\nu}X$ [20]. This component is estimated using $\mathcal{B}(B \to D_s^{(*)}K\mu^-\overline{\nu}) = (6.1 \pm 1.2) \times 10^{-4}$ recently measured by the BaBar collaboration [20]. Finally, Λ_b's decay mostly into Λ_c final states. We search for other Λ_b contributions using $D^0pX\mu^-\overline{\nu}$ events. Additional b-baryon final states are assumed to be at the level of 10% of the Λ_b contribution and are not looked for directly. We also ignore the contributions of $b \to u$ semileptonic decays that constitute approximately 1% of semileptonic decays [7].

In order to evaluate the efficiencies we need to simulate a proper mix of the semileptonic decays of all the b-hadron species. The semileptonic decay modes of the light B mesons were generated according to the tables shown in a separate note [8]. For the B_s and Λ_b we generated individual exclusive modes and averaged the efficiencies depending on the mix of final states expected on the basis of an exclusive reconstruction analysis discussed later.

Our goals are to measure two specific production ratios. The first is that of B_s relative to the sum of B^- and $\overline{B}^0$. We denote the individual hadron fractions as f_s, f_u and f_d, where the subscript reflects the identity of the spectator anti-quark in the meson. For Λ_b we use f_{Λ_b}. Note that the sum of these f's does not equal one as there is other b production, including a very small rate for B_c mesons and other b-baryons, that do not decay strongly into Λ_b. The baryon with the largest rate we are missing is the Ξ_b. In principle we could search for these using $\Xi_cX\mu^-\overline{\nu}$ final states, but even if we found them we could not infer a rate since branching fraction measurements of Ξ_c final states do not exist.

The number of $\overline{B}_s^0$ resulting in $D_s^+X\mu^-\overline{\nu}$ in the final state is given by

$$\begin{aligned} n_{\rm corr}(\overline{B}_s^0 \to D_s^+\mu) &= \frac{n(D_s^+\mu)}{\mathcal{B}(D_s^+ \to KK\pi)\epsilon(\overline{B}_s^0 \to D_s^+\mu)} - \\ & \quad N(\overline{B}^0 + B^-)\mathcal{B}(B \to D_s^+K)\frac{\epsilon(\bar{B} \to D_s^+K\mu)}{\epsilon(\overline{B}_s^0 \to D_s^+\mu)} \end{aligned} \tag{1}$$

where the last term subtracts yields of $D_s^+KX\mu^-\overline{\nu}$ final states originating from $\overline{B}^0$ or B^- semileptonic decays, and $N(\overline{B}^0 + B^-)$ indicates the total number of $\overline{B}^0$ and B^- produced. We derive this correction using the BaBar branching fraction $\mathcal{B}(B \to D_s^{(*)}K\mu\nu) = (6.1 \pm 1.2) \times 10^{-4}$ [20]. In addition, $\overline{B}_s^0$ decays semileptonically into $DKX\mu^-\overline{\nu}$, and thus we need to add to Eq. 1

$$n_{\rm corr}(\overline{B}_s^0 \to DK^+\mu^-) = 2\frac{n(D^0K\mu)}{\mathcal{B}(D^0 \to K\pi)\epsilon(\overline{B}_s^0 \to D^0K\mu)}, \tag{2}$$

where we have used isospin symmetry to account for $\overline{B}_s^0 \to D^+KX\mu^-\overline{\nu}$ semileptonic decays.

The equation for the ratio $f_s/(f_u+f_d)$ is

$$\frac{f_s}{f_u+f_d} = \frac{n_{\rm corr}(\overline{B}^0_s \to D\mu)}{n_{\rm corr}(B\to D^0\mu)+n_{\rm corr}(B\to D^+\mu)}\frac{\tau_{B^-}+\tau_{\overline{B}^0}}{2\tau_{\overline{B}^0_s}}. \tag{3}$$

where $\overline{B}^0_s \to D\mu^-\overline{\nu}$ represents $\overline{B}^0_s$ semileptonic decays to a final charmed hadron, given by the sum of the contributions shown in Eqs. 1 and 2, and τ_{B_i} indicates the B_i hadron lifetime; they are all well measured. This equation assumes equality of the semileptonic widths of all the b meson species. This is a fairly reliable assumption, as corrections in HQET arise only to order $1/m_b^2$ and the SU(3) breaking correction is quite small, of the order of 1% [9, ?, 11].

The Λ_b corrected yield is derived in an analogous manner. We determine

$$n_{\rm corr}(\Lambda_b\to D\mu) = \frac{n(\Lambda_c^+\mu^-)}{\mathcal{B}(\Lambda_c^+\to pK^-\pi^+)\epsilon(\Lambda_b\to\Lambda_c)} + 2\frac{n(D^0p\mu)}{\mathcal{B}(D^0\to K^-\pi^+)\epsilon(\Lambda_b\to D^0p)}, \tag{4}$$

where D represents a generic charmed hadron, and extract the Λ_b fraction using

$$\frac{f_{\Lambda_b}}{f_u+f_d} = \frac{n_{\rm corr}(\Lambda_b \to D\mu)}{n_{\rm corr}(B\to D^0\mu)+n_{\rm corr}(B\to D^+\mu)}\frac{\tau_{B^-}+\tau_{\overline{B}^0}}{2\tau_{\Lambda_b}}, \tag{5}$$

Here again we assume near equality of the semileptonic widths of the different b-hadrons, but we apply a small correction of (4±2)%, to account for the fact that baryon species are not affected by the chromo-magnetic correction [9, 10, 11].

I.a Rationale for the equality of semileptonic widths of b-flavored hadrons

The formulae for the b-fractions are derived assuming equality of all the b hadron semileptonic widths $\Gamma_{\rm sl}$. In HQET this statement is valid up to $1/m_b^2$ corrections [9],[10]. These corrections are expected to amount at most to a few percent. To be more precise, corrections to order $1/m_b^2$ include the kinetic term, which we denote as K_b, using the notation of Ref. [9], and the chromomagnetic operator, which we denote as G_b. The latter operator affects only b-flavored mesons. The kinetic term is very similar for all the hadrons studied in this analysis, for example, Manohar and Wise [9] estimate $K_b(\Lambda_b)-K_b(B) = -0.002\pm0.006$. The chromomagnetic operator, affecting only b-flavored mesons, and not the Λ_b, is related to the mass splitting between B^* and B mesons

$$m_bG_b(B) = -\frac{3}{4}[M(B^*)-M(B)], \tag{6}$$

where m_b is the b quark mass. The measured $M(B^*)-M(B)$ is 45.78±0.35 MeV for $\overline{B}^0$, B^-, and 49.0±1.5 MeV for B_s. As these mass splittings are nearly identical, this correction is essentially the same for the $\overline{B}^0_s$, $\overline{B}^0$, and B^- mesons. Finally, these operators enter the general expression for the inclusive semileptonic width with phase space coefficients, related to $\rho \equiv m_c^2/m_b^2$. The expression for the inclusive semileptonic width has been evaluated independently in Ref. [9], and Ref. [10] up to $1/m_b^2$ terms and is given by

$$\frac{\Gamma(B)}{\Gamma_b} = [1 - 8\rho + 8\rho^3 - \rho^4 - 12\rho^2 \log\rho] + (K_b + E_b)[5 - 24\rho + 24\rho^2 - 8\rho^3 + 3 - 12\rho^2 \log\rho] + \tag{7}$$

$$K_b[-6 + 32\rho - 24\rho^2 - 2\rho^4 + 24\rho^2 \log\rho] + G_b[-2 + 16\rho - 16\rho^3 + 2\rho^4 + 24\rho^2 \log\rho] \tag{8}$$

Using the central values $m_c = 1.27$ GeV and $m_b = 4.62$ GeV, and applying conservative errors, we derive $[\Gamma(\Lambda_b) - \Gamma(B)]/\Gamma(B) = (4 \pm 2)\%$. We include this correction in our estimate $f_{\Lambda_b}/(f_u + f_d)$.

2 Signal extraction

II.a Common selection criteria

Most charm hadrons are produced directly via $pp \to c\overline{c}X$ interactions, where the X indicates the sum over all other possible final state particles. We denote these particular charm decays as "Prompt". Charm can also be produced in $pp \to b\overline{b}X$ collisions where the b-flavored hadron decays into charm. We call these charm from b's or "Dfb" for short.

We use common selection criteria for all the decay modes. They are specified in Table 2. This analysis closely mirrors our previous analysis of $b \to D^0 X \mu^- \overline{\nu}$ [4]. The criteria for the other modes are similar. We specify TOS on the single muon.

Table 2: Selection criteria

Item	requirement
Muon identification	
Track fit	χ^2/ndof<5
Minimum IP	$\chi^2 > 4$
Momentum	$p > 3$ GeV
Transverse momentum	$p_t > 1200$ MeV
ISMUON	OK
DLL($\mu - \pi$)	> 0
N shared hit	=0
Hlt1	SingleMuonNoIP
Hlt2	SingleMuon
Charm hadron daughters	
Track fit	χ^2/ndof<5
Minimum IP	$\chi^2 > 9$
Momentum	$p > 2$ GeV
Transverse momentum	$p_t > 300$ MeV
Particle Identification for pions	DLL($K - \pi$) < 10
Particle Identification for kaons	DLL($K - \pi$) > 4
Particle Identification for protons	DLL($p - \pi$) > 10 and DLL($p - K$) > 0
Charm hadron selection	
Sum p_t of daughters/# of daughters	> 700 MeV
vertex χ^2/ndof	< 6
Flight Distance χ^2	> 100
IP	<7.4 mm i.e. ln(IP/mm)<2
DIRA	> 0.9
***b* selection criteria**	
b vertex χ^2/ndof	< 6
b DIRA	> 0.999
Charm vertex downstream of b vertex	z(charm)-z(b)> 0
η	$2 < \eta < 6$
Invariant mass of $D^0(D^+)$ + muon	$3 < m(D^0 + \mu) < 5$ GeV
Invariant mass of D_s^+ + muon	$3.1 < m(D_s^+ + \mu) < 5.1$ GeV
Invariant mass of Λ_c + muon	$3.3 < m(\Lambda_c + \mu) < 5.3$ GeV

The additional criteria imposed when searching for $D^0K^+X\mu^-\overline{\nu}$ or $D^0pX\mu^-\overline{\nu}$ candidates are listed in Table 3.

Table 3: Additional selection criteria when including another hadron

Item	**requirement**
Criteria for $D^0K^+X\mu^-\overline{\nu}$ events	
IP of D^0 candidate	> 0.05 mm (ln(IP/mm)>-3)
K^+ tracking	$\chi^2_{\rm IP} > 9$, $p_t > 300$ MeV, Clone track rejection (CloneDist$\leq$0)
K^+ PID	DLL$(K-\pi) > 4$, DLL$(K-p) > 0$
D^0K^+ transverse momentum	> 1.5 GeV
b mass	$3.09 < m(D^0K^+\mu^-) < 5.09$ GeV
b vertex χ^2/ndof	< 3
b DIRA	> 0.999
z(charm+K)-z(b)	> 0
D^{*+} rejection	$m(K^-\pi^+\pi^+) - m(K^-\pi^+) - m(\pi^+) > 20$ MeV
Criteria for $D^0p^+X\mu^-\overline{\nu}$ events, same as above except	
p PID	DLL$(p-\pi) > 10$ and DLL$(p-K) > 0$
b mass	$3.3 < m(D^0p\mu^-) < 5.3$ GeV

The Prompt and Dfb components can be separated statistically by examining the impact parameter (IP) with respect to the primary vertex, where IP is defined as the smallest distance between the charm hadron direction and primary vertex position.

To isolate a relatively background free sample of B mesons we match D candidates with tracks identified as muons. Right-sign (RS) combinations have the sign of the charge of the muon being the same as the charge of the kaon in the D decay. Wrong-sign (WS) combinations have the sign of the charge of the kaon and the muon being the opposite.

The data used here were taken with a maximum number of average interactions per crossing at the start of the run of 1.5. Nevertheless, there are events with large numbers of long tracks. Backgrounds do increase with increasing track numbers. In Fig. 1 we plot the $K^-\pi^+$ mass for events with a RS muon satisfying the criteria in Table 2 as a function of the number of long tracks in the crossing. The data are fitted with a double-Gaussian signal function, with both Gaussians having the same mean, and a linear background. This signal shape is used in all subsequent fits. Note that the Gaussian σ does not depend upon the number of tracks in the event (the fit results are: 7.46$\pm$0.05 MeV for events with less than 50 tracks, 7.47$\pm$0.09 for events with a number of tracks between 50 and 99, 7.49$\pm$0.24 MeV for events with 100 to 149 tracks, 8.3$\pm$0.7 MeV for events with 150 to 199 tracks, and 7.0$\pm$1.2 MeV for events with 200 tracks or more. We select $K^-\pi^+$ candidates within $\pm$20 MeV of the fitted D^0 mass.; the signal/background ratio is shown in the lower right hand corner. It decreases by about a factor of ten over the range considered here.

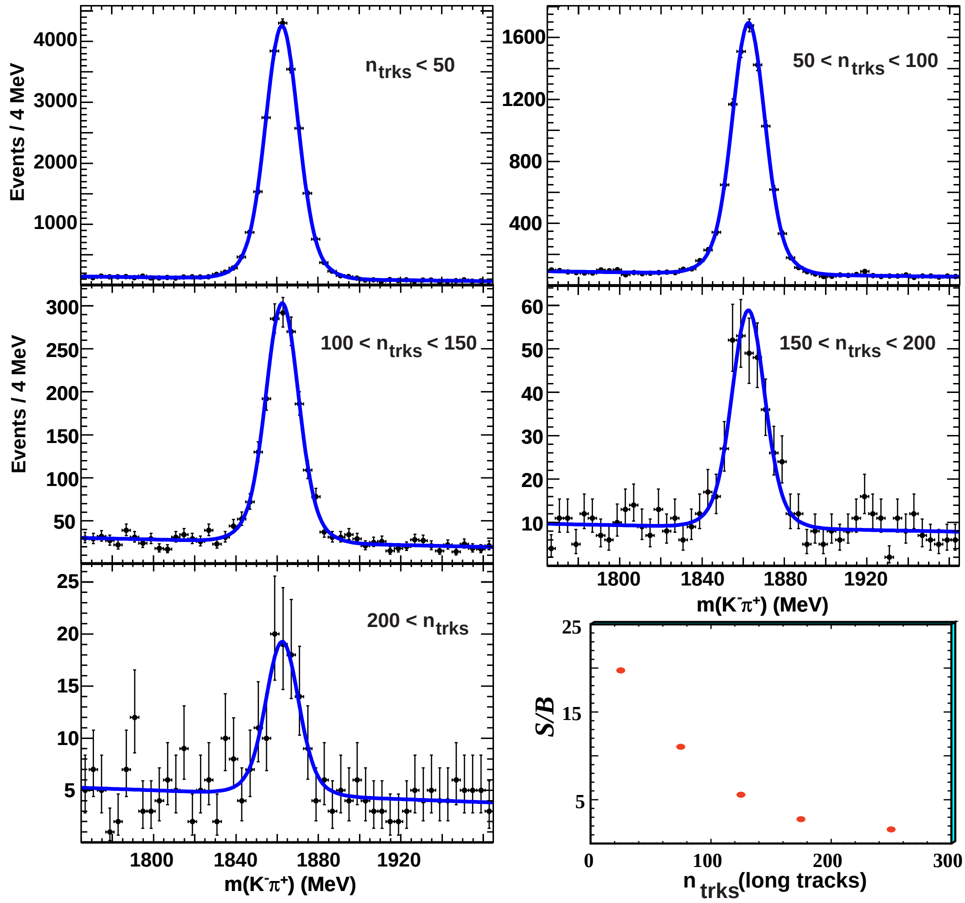

Figure 1: The $K^-\pi^+$ invariant mass distributions as a function of the number of long tracks in the crossing. In the lower right corner the signal/background ratio is shown.

We show the ln(IP/mm) distributions for these events that are within ±20 MeV of the D^0 mass in Fig. 2. The fake background rise is apparent. We list in Table 4 the results of these fits.

Table 4: Yields for $B \to D^0 X \mu^- \overline{\nu}$ as a function of the number of long tracks.

# long tracks	Dfb	Prompt	Fake D^0	S/B≡Dfb/Fake	σ_M(MeV)
0-50	20759±150	248±32	1052±17	19.7±0.4	7.46±0.05
50-100	804±95	146±22	732±14	11.0±0.2	7.47±0.09
100-150	1382±38	26±10	24 ±7	5.6±0.2	7.49±0.24
150-200	244±17	9±5	88±4	2.8±0.1	8.3 ±0.7
≥200	73±11	1±3	45±3	1.6±0.3	7.0±1.2

Since signals in the other D channels are not as clean as in the D^0 channel we impose

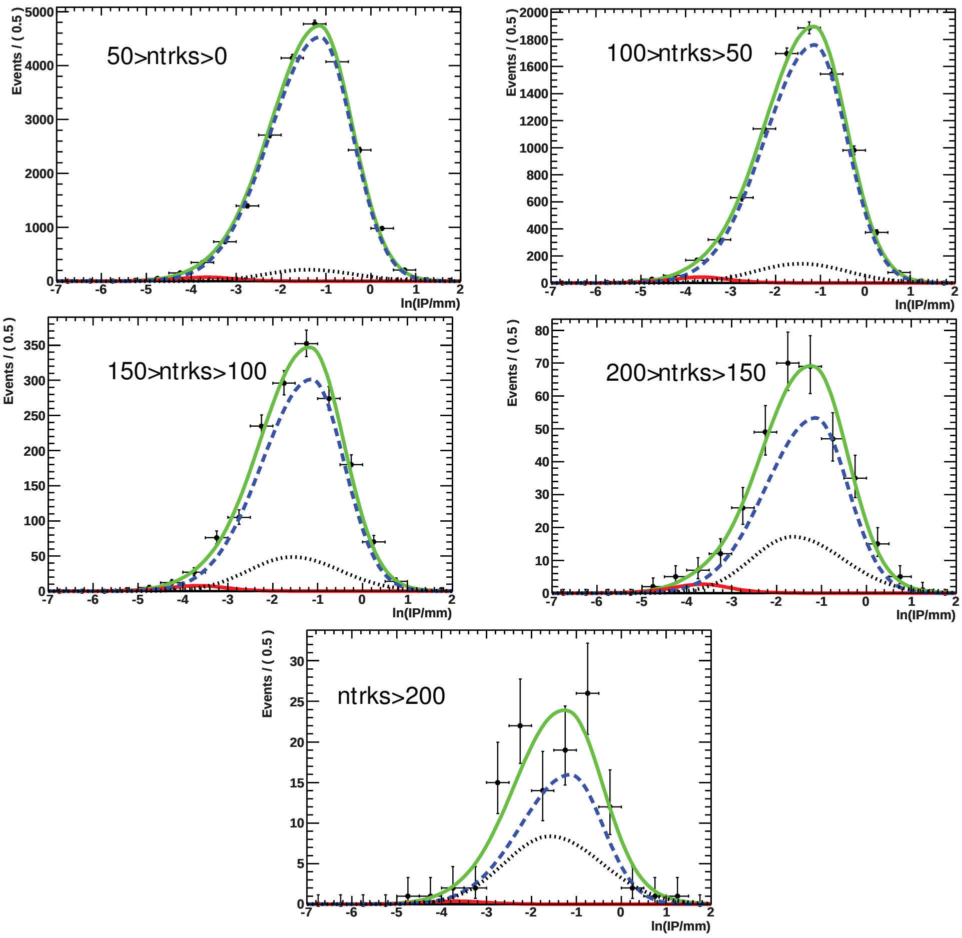

Figure 2: The Logarithm of the IP distributions for RS D^0 candidate combinations with a muon for different intervals of long tracks in the crossing. The dotted curves show the sideband backgrounds, the small solid curves the Prompt yields, the dashed curve the Dfb signal, and the larger solid curves the totals.

the additional requirement that the number of long tracks be less than 100. This results in only a 5.6% loss of signal.

II.b The $D^0 X\mu^-\overline{\nu}$ final state

In order to extract the $D^0 X\mu^-\overline{\nu}$ raw yield, we perform an unbinned extended maximum likelihood to the two-dimensional distributions in $K^-\pi^+$ invariant mass over a region extending $\pm$80 MeV from the D^0 mass peak, and ln(IP/mm). This fitting procedure allows us to determine the background shape from false combinations under the D^0 signal mass peak directly. The parameters of the Prompt IP distribution are found by examining directly produced charm [4]. The Monte Carlo simulated shape is used for the Dfb component. Both the RS and WS $K^-\pi^+$ mass spectra as well as fits to Logarithm of (IP/mm) distributions for events with mass combinations within $\pm$20 MeV of the D^0 mass are shown in Fig. 3.

The fits are quite good. The RS fitted yields are 27666$\pm$187 Dfb, 695$\pm$43 Prompt, and 1492$\pm$30 D^0 combinatoric background. For WS we find 362$\pm$39 Dfb, 187$\pm$18 and 1134$\pm$19 false D^0 combinations. As this paper focuses only on ratios of yields, we do not explicitly make the $\approx$0.5% subtraction to the RS $DX\mu^-\overline{\nu}$ yields. The Dfb number in the WS is consistent with what is expected from hadron to muon fakes. Since we are taking ratios of yields in this paper and since the fake fraction is virtually the same for hadrons to muons independent of the charm hadron, we do not explicitly make the $\approx$0.5% muon fake subtraction to the RS $DX\mu^-\overline{\nu}$ yields.

II.c The $D^+ X\mu^-\overline{\nu}$ modes

We use the same fitting method to derive the Dfb raw yields from the study of the Logarithm of (IP/mm) and M($K^-\pi^+\pi^-$) for [($D^+ \to K^-\pi^+\pi^-$)-μ] candidates satisfying our selection criteria. In Fig. 4 we show the Logarithm of (IP/mm) and $K^-\pi^+\pi^+$ invariant mass combinations for events with muon candidates. The extracted numbers of these $D^+ X\mu^-\overline{\nu}$ for the b direction in $2 < \eta < 5$ are 9257$\pm$111 Dfb events, 362$\pm$34 Prompt, and 1150$\pm$22 in the D^+ sideband regions, that reflects the background under the signal mass peak. For WS we find 77$\pm$22 Dfb, 139$\pm$14 Prompt and 307$\pm$10 in the D^+ sideband regions.

Both the $D^0 X\mu^-\overline{\nu}$ and the $D^+ X\mu^-\overline{\nu}$ final states contain a small component of cross feed from $\overline{B}^0_s$ decays to $D^0 K^+ X\mu^-\overline{\nu}$ and $\overline{B}^0_s$ decays to $D^+ K^0 X\mu^-\overline{\nu}$. This component is accounted for by the two decays $\overline{B}^0_s \to D_{s1} X\mu^-\overline{\nu}$ and $\overline{B}^0_s \to D^*_{s2} X\mu^-\overline{\nu}$ and has been reported in a recent LHCb publication [12].

II.d The $D_s X\mu^-\overline{\nu}$ modes

The analysis for the $D_s^+ X\mu^-\overline{\nu}$ mode follows in the same manner. Here, however, we are concerned about the reflection from $\Lambda_c \to pK^-\pi^+$ where the proton is taken as kaon, since we do not have an explicit proton veto. Using such a veto would lose 30% of the

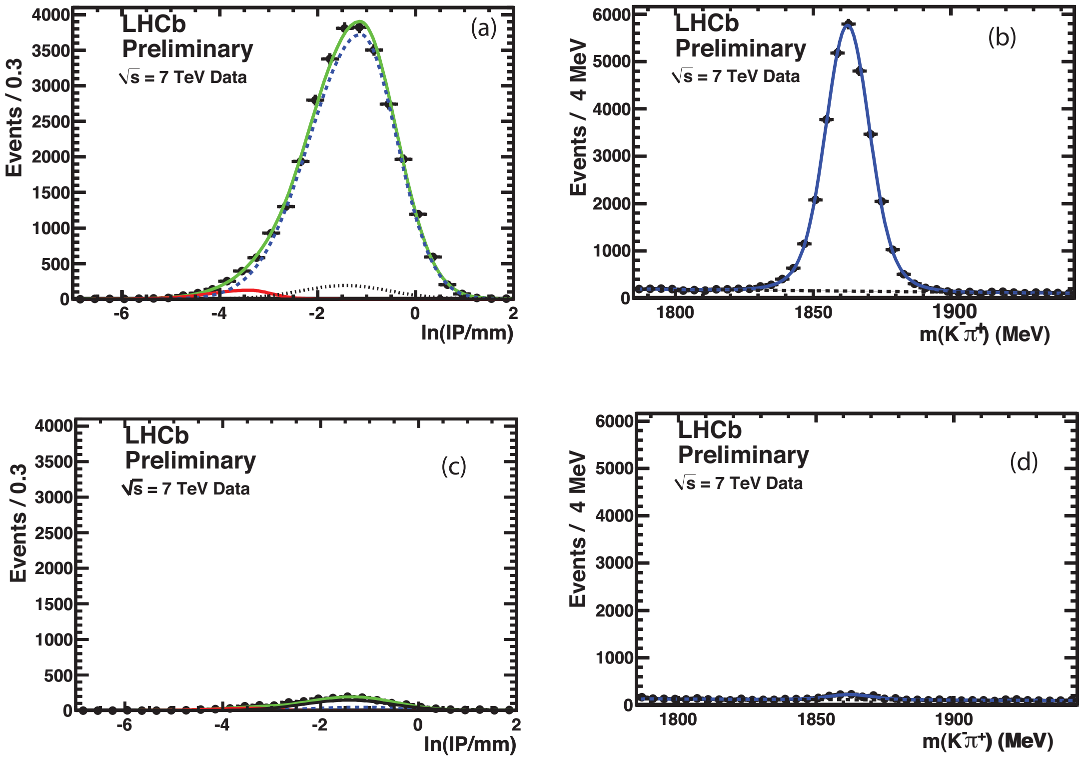

Figure 3: The Logarithm of the IP distributions for (a) RS and (b) WS D^0 candidate combinations with a muon within the $\pm$ 20 MeV mass region: the dotted curves show the sideband backgrounds, the small solid curves the Prompt yields, the dashed curves the Dfb signal, and the large solid curves the totals. The invariant $K^-\pi^+$ mass spectra for RS combinations (c) and WS combinations (d) are also shown.

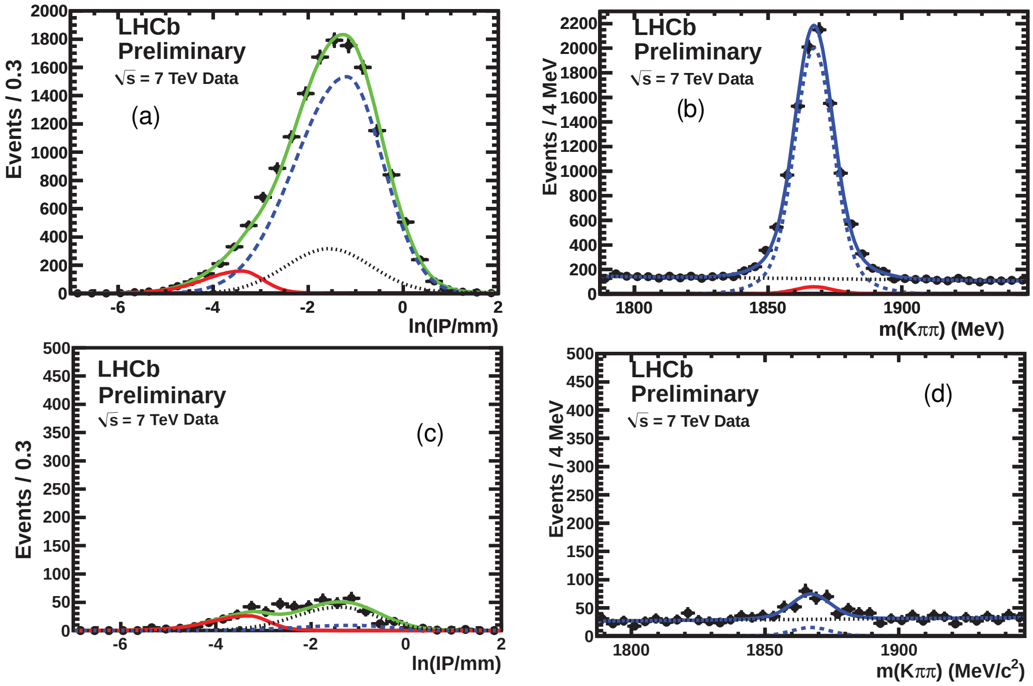

Figure 4: The Logarithm of the IP distributions for (a) RS and (c) WS D^+ candidate combinations with a muon. The grey-dotted curves show the sideband backgrounds, the small red-solid curves the Prompt yields, the blue-dashed curves the Dfb signal, and the larger green-solid curves the totals. The invariant $K^-\pi^+\pi^+$ mass spectra for RS combinations (c) and WS combinations (d) are also shown.

signal and introduce a systematic error. We choose to model separately this particular background. In Fig 5 we show the Monte Carlo simulated $\Lambda_b \to \Lambda_c X \mu^- \overline{\nu};\ \Lambda_c \to pK^-\pi^+$ signal events when the p is assigned to be a K^+. The shape of the reflection is determined from simulation and its normalization is allowed to float within the error of our calculation of the size of the background.

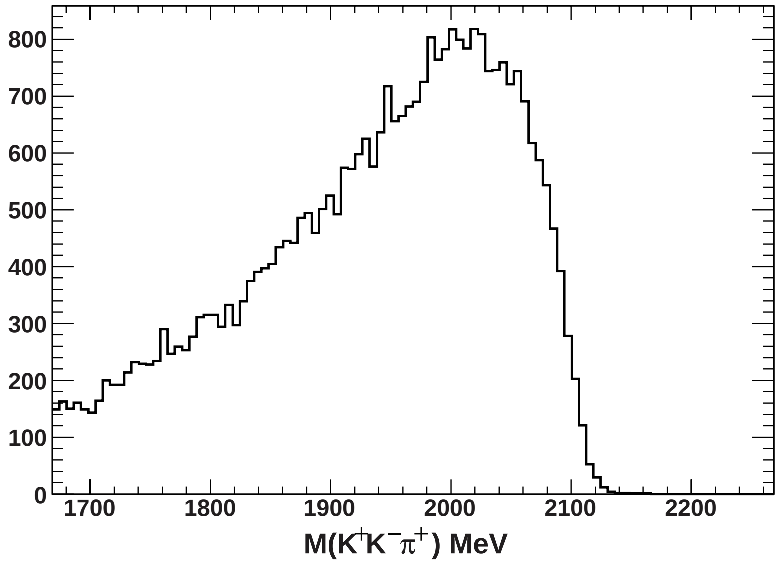

Figure 5: Monte Carlo simulated $\Lambda_b \to \Lambda_c X \mu^- \overline{\nu};\ \Lambda_c \to pK^-\pi^+$ signal events when the p is assigned to be a K^+.

We use the shape of this distribution as an additional probability density function (PDF) that we add in the fit. We show in Fig. 6 the Logarithm of (IP/mm) and $K^-K^+\pi^+$ invariant mass combinations for events with muon candidates. We use the shape of this distribution as an additional probability density function (PDF) that we add in the fit. Finally, we include a component modeling the background from $D^{*+} \to \pi^+ D^0$ with D^0 decaying into K^+K^-. Fig. 6 shows the Logarithm of (IP/mm) fit projection, for $KK\pi$ candidate mass within the D_s signal window, and the $KK\pi$ invariant mass projection. The measured yields in the RS sample are 2192±64 Dfb, 53±16 Prompt, 985±145 combinatoric, 387±132 Λ_c reflection background, 3.5±0.5 D^{*+}, the corresponding yields in the WS sample are 13.3±19, 20±7.3, 499±16, 3±3, 0±0.1. If we leave out the additional PDF for the Λ_c reflection, we find the signal yield increases by 2.3%.

II.e The $\Lambda_c \mu^- \overline{\nu} X$ final state

To complete our charm candidates, we study the final state Λ_c Fig. 7 shows the data and fit components to the Logarithm of (IP/mm) and $pK^-\pi^+$ invariant mass combinations for events with $2 < \eta < 5$. This fit gives 3028±112 RS Dfb events, 43±17 RS Prompt events, 589±27 RS sideband events, 9±16 WS DfB events, 0.5 ±4 WS Prompt events, and 177±10 WS sideband events.

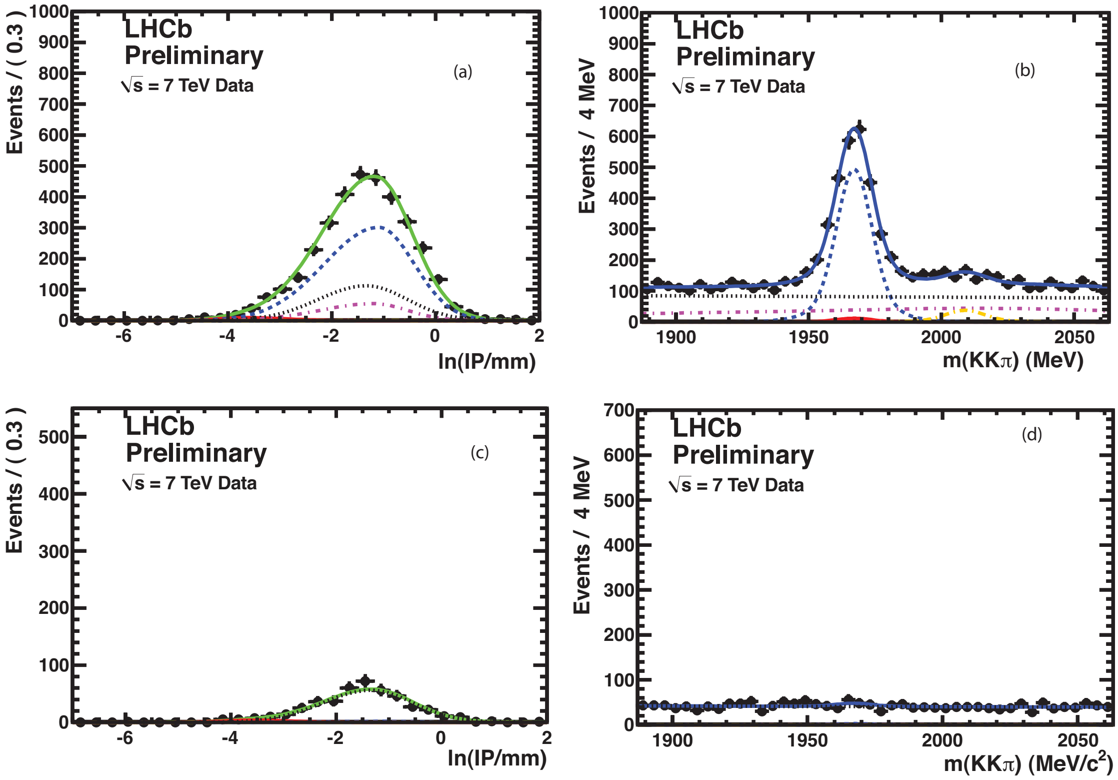

Figure 6: The Logarithm of the IP distributions for (a) RS and (c) WS D_s candidate combinations with a muon. The grey-dotted curves show the sideband backgrounds, the small red-solid curves the Prompt yields, the blue-dashed curves the Dfb signal, the purple dash-dotted curves represent the background originating from Λ_c reflection, and the larger green-solid curves the totals. The invariant $K^-K^+\pi^+$ mass spectra for RS combinations (b) and WS combinations (d) are also shown.

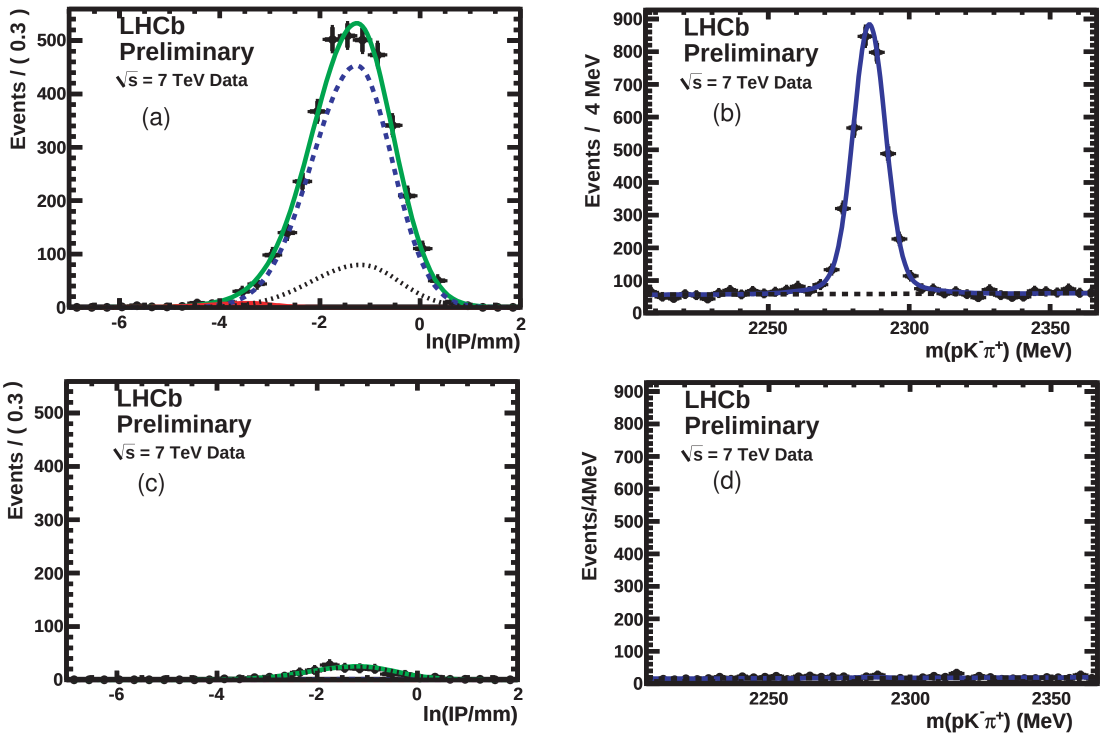

Figure 7: The Logarithm of the IP distributions for (a) RS and (c) WS Λ_c^+ candidate combinations with a muon. The grey-dotted curves show the sideband backgrounds, the small red-solid curves the Prompt yields, the blue-dashed curves the Dfb signal, and the larger green-solid curves the totals. The invariant $p^- K^- \pi^+$ mass spectra for RS combinations (b) and WS combinations (d) are also shown.

3 Measurement of $D^0 K^+ X \mu^- \overline{\nu}$

Semileptonic decays of $\overline{B}{}^0_s$ mesons usually result in a D_s^+ meson in the final state. It is possible, however, that the semileptonic decay goes to an excited D_s^{**+}, which can decay into either DK or D^*K final states. Resonance formation is not required, these can just be produced via fragmentation. To ascertain the size of this effect we measure the $D^0 K^+ \mu^- \overline{\nu}$ yield. We then double this to account for the $D^+ K^0 X \mu^- \overline{\nu}$ that are equal by isospin conservation. Fig. 8 shows the $D^0 K^+$ invariant mass spectrum. D^0 candidates were chosen from $K^+ \pi^- X \mu^- \overline{\nu}$ events with a $K^- \pi^+$ invariant mass within ± 20 MeV of the D^0 mass.

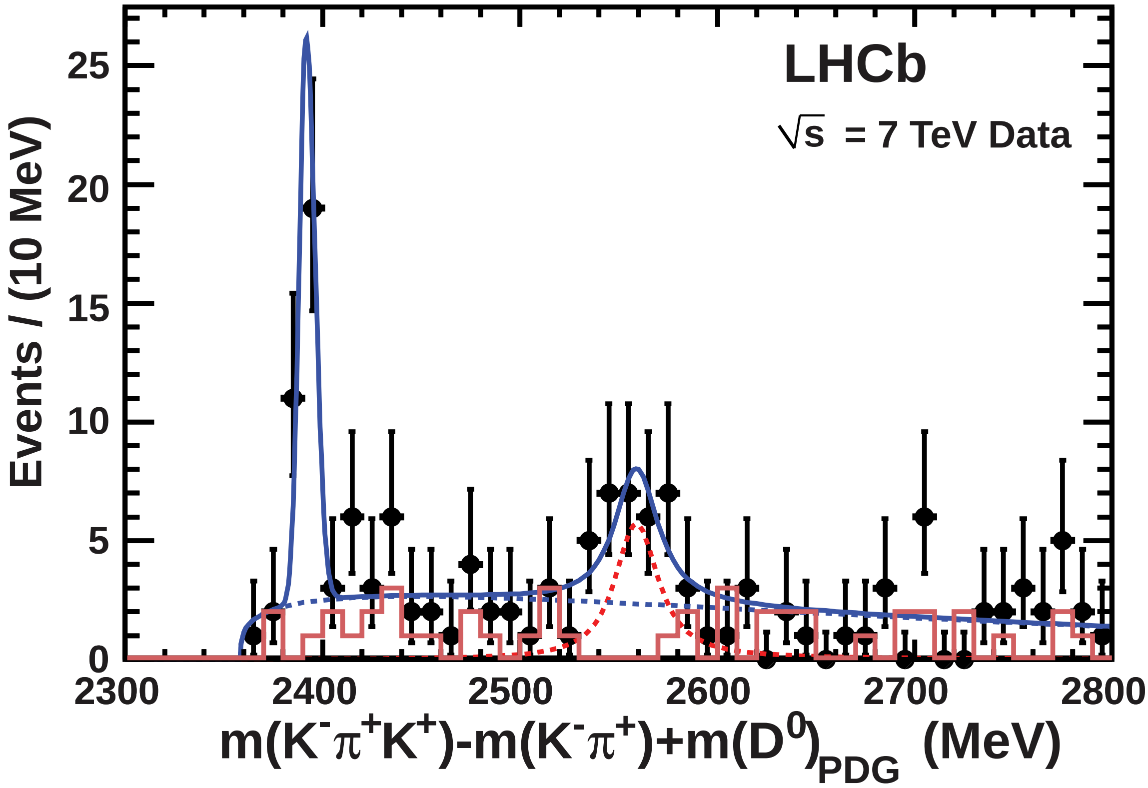

Figure 8: The mass difference $(K^- \pi^+ K^+)$-$(K^- \pi^+)$ added to the known D^0 mass for events with $K^- \pi^+$ invariant masses within ± 20 MeV of the D^0 mass (black points) in semileptonic decays using the 3 pb^{-1} data sample. The histogram shows events with an additional K^- instead of a K^+ and thus are of wrong sign of charge to come from a single semileptonic decay. The curves are described in the text.

A clear narrow signal is seen for the $D_{s1}^+(2536)$. This resonance decays exclusively into $D^{*0}K^+$ and $D^{*+}K^0$. Because it is so close to threshold our mass resolution is very good even though the γ or π^0 is not reconstructed. This final state was seen previously in $\overline{B}_s^0$ semileptonic decays by the D0 collaboration where the $D_{s1}^+ \to D^{*+}K_s$ [13]. There also appears to be a feature near the known mass of the $D_{s2}^{*+}(2573)$, although there is not sufficient data in this sample to conclude that we have made a new observation. In what follows we use a much larger sample for this state.

Next we investigate the two possibly resonant structures. The wider one is close to the D_{s2}^{*+} mass of 2573 MeV. Its width is not well measured; the PDG quotes 20±5 MeV [1]. We simulate the decay of the narrower structure. Fig. 9 shows the Monte Carlo generated mass of the D^0 plus K^+, $m(D^0K^+)$ from $D_{s1}^+ \to D^{*0}K^+$ with the D^{*0} subsequently decaying into a γ or π^0 and a D^0, where we do not include the γ or π^0 in the reconstruction. Fig. 9 shows also the fit to MC data, implemented with a bifurcated Gaussian that is used only to constrain the ratio between the high side/low side widths. It predicts a mass value 2392.2 MeV and a width of 4.2 MeV, while the known D_{s1}^+ is 2536 MeV; the reconstructed value us lower because of the missing particle.

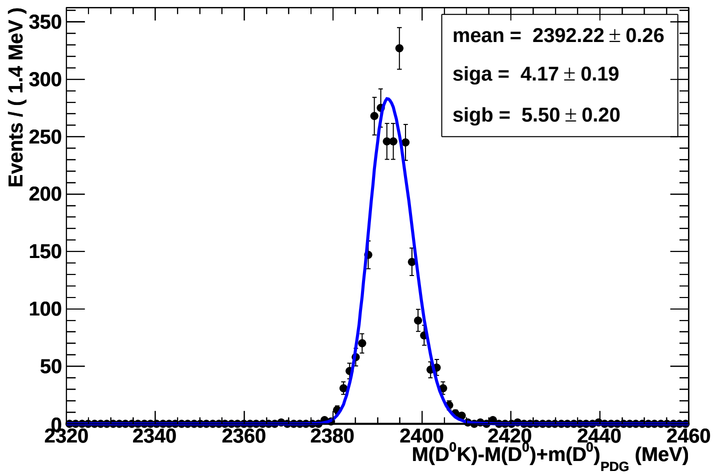

Figure 9: $m(D^0K^+)$ for $D_{s1}^+ \to D^{*0}K^+$ decays. The fit is to a bifurcated Gaussian whose mass and width values are shown.

In order to ascertain the size of the putative signals above background we perform an unbinned maximum likelihood fit. The data are fit to a threshold background function proportional to $[m(D^0K^+) - m_0]^p e^{-a*[m(D^0K^+)-m_0]}$, where m_0, the threshold point is fixed at 2358.52 MeV. The fit determines p and a. For the D_{s1}^+ signal function we use the bifurcated Gaussian shape, whose width ratio is determined from MC. The mass and width(average of the two widths in the bifurcated Gaussian) are fixed to the values of 2391.6 MeV and 3.5 MeV respectively, derived from fits to the higher statistics data sample discussed below. The simulation, including the effects of the missing D^{*0} decay product, predicts a mass of 2392.2±0.3 MeV and a width of 4.2±0.2 MeV. There are 24.4±5.5

D_{s1}^{+} events. A relativistic Breit-Wigner signal shape convoluted with the experimental resolution of 3.3 MeV (r.m.s., from MC) is used in the region of the D_{s2}^{*+} where both the mass and width are allowed to float in the fit. We find a mass value of 2559±9 MeV, a width of 25.2±9.2 MeV and 22.2±7.5 events. The fit is not sensitive to whether we assume a spin 0 or a spin 2 Breit-Wigner resonance shape. The sum of the yields from these two resonances is 47±9.3±4.7. Thus we do not see any evidence for a non-resonant component in this mass region.

The Breit-Wigner form used is given by

$$BW(m) = \frac{m\Gamma(m)}{(m^2 - m_0^2)^2 + [m_0\Gamma(m)]^2}, \tag{9}$$

where m is the D^0K^+ mass for each event and m_0 is the resonance mass that we are fitting for.

In order to assess the magnitude of a possible non-resonant signal component, we study the RS/WS ration in signal and MC. We use Monte Carlo simulation to give us an estimate of the expected backgrounds. Two sources are evident: one is fake kaons that the wrong-sign estimates well, and the other is fakes from kaons from the other b decay in the event. From MC we derive a predicted ratio RS/WS background = 1.8± 0.4. In addition, RS and WS yields are obtained by fitting the D^0 mass peaks for events where an additional K is found and excluding the regions where resonant structures are seen: [2360,2410] MeV (D_{s1}^{+}), and [2520,2610] MeV (D_{s2}^{*+}). The fits are shown in Fig. 10. The RS and WS yields are 78±10 events and 47±8, with a corresponding ratio RS/WS = 1.7±0.4, consistent with predicted background. In order to assess the systematic error on the number of $D^0K\mu^-\overline{\nu}X$ associated with the errors in the data and MC RS/WS yields, we use a toy MC to predict the non-resonant contribution in the peak vetoed regions, using the measured values of RS and WS events in the non-excluded region, and the data and MC RS/WS ratios and their errors to obtain 0^{+17}_{-0} non-resonant signal events. This gives a $\overline{B}_s^0 \to D^0K\mu^-\overline{\nu}X$ yield of $47\pm9^{+18}_{-5}$ events. In the $2 \leq \eta \leq 5$ interval, the corresponding yield is $39\pm10^{+18}_{-5}$ events.

4 Measurement of $D^0pX\mu^-\overline{\nu}$

Here we select events in a similar manner as in D^0K^+ but now insist that the charged track is identified as a proton. (For specific selection criteria see Table 2.) The resulting D^0p invariant mass distribution is shown in Fig. 11. We also show the combinations that cannot arise from Λ_b decay, namely those with $D^0\overline{p}$ combinations. There is a clear excess of RS over WS combinations especially near threshold. We find 152±13 RS events, and 55±8 WS events. Using the ratio between the RS and WS background events predicted by MC (1.39±0.2), we find 75±17±11 events that come from Λ_b decays, where the systematic error is given by the error on the background estimate.

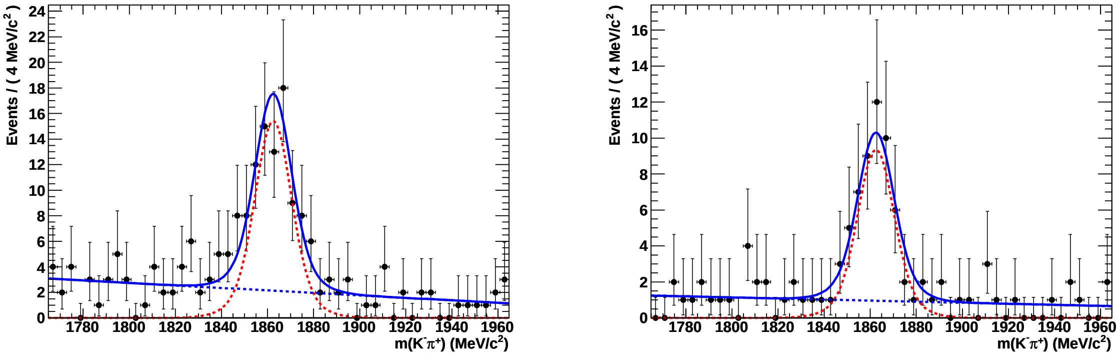

Figure 10: Invariant mass of the $K^-\pi^+$ combination in the [M(D^0K) $- M(D^0)$] signal region with the resonance interval excluded from the projection (for details see text): the left plot corresponds to the RS combinations and the right plot corresponds to the WS combination. The red dashed curves correspond to the signal region.

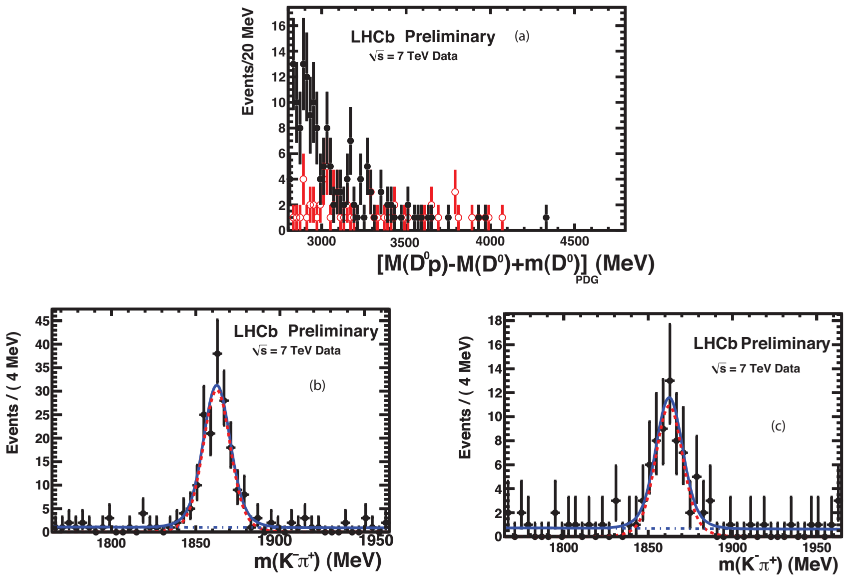

Figure 11: Invariant mass of D^0p candidates that vertex with each other and together with a RS muon (black closed points) and for a $\overline{p}$ (red open points) instead of a p (a); fit to D^0 invariant mass for RS events with the invariant mass of D^0p candidate in the signal mass difference window (b); fit to D^0 invariant mass for WS events with the invariant mass of D^0p candidate in the signal mass difference window (c).

5 Observation of $\overline{B}^0_s \to D^{*+}_{s2}(2573)X\mu^-\overline{\nu}$

To see if the D_{s2} signal is real requires more data. Using the sum of Stripping09 and Stripping10 we have approximately 20 pb^{-1} available, where we accept all triggered events that are stripped. Fig. 12 shows the resulting invariant mass spectrum. The obvious resonant peaks are fit in the same way as in the 3 pb^{-1} data sample. We fit the D^+_{s1} peak with a bifurcated Gaussian shape, whose relative widths above and below the peak are determined from MC. The fit to the D^+_{s1} gives 2391.6±0.5 MeV for the mass, 4.0±0.4 MeV for the width, and yields 155±15 signal events. For the D^{*+}_{s2} we again allow the mass, the width and the number of events to float in the fit. We find a mass of 2569.4±1.6 MeV, a width of 12.1±4.5 MeV, and 82±17 events. These errors are purely statistical. The previously measured mass and width values from the PDG are 2572.6±0.9 MeV, and 20±5 MeV [1]. The probability of the background fluctuating to form the D^{*+}_{s2} signal corresponds to 8 standard deviations. Note that the D0 collaboration could not observe the D^{*+}_{s2} in their $D^{*+}K_s$ search since the only observed decays are to DK final states. Fig. 13 shows the yield in the D^0 sidebands regions, selected on both sides of the D^0 peak, in the intervals between 45 and 75 MeV away from the D^0 mass.

In order to confirm that the fit does not bias the mass and width of the D^{*+}_{s2}, we have used 350 toy MC samples, with the inputs obtained from the 20 pb^{-1} data. Figs 14 and 15 show the corresponding distributions of masses and widths returned from the fits. No bias is discernible. The pulls of these distributions are 1.06±0.04 for the mass and 0.94±0.05 for the width.

The systematic error on the D^{*+}_{s2} mass is determined by looking at several calibration channels. For example, our measured D^0 differs from the known value by 0.2 MeV, though the known value has a 0.14 MeV error. The MC determined resolution does not affect the systematic error. We also see a variation on the order of 0.3 MeV by varying the fit region and background shape (linear, threshold). The baseline fit region is the interval (2300,2800) MeV, alternatively we use a more restricted interval of (2370,2800) MeV. Thus we take ±0.5 MeV as the systematic uncertainty. We use the same method of changing the fits to find the systematic uncertainty on the width. The maximum observed change is 1.4 MeV, that we take as the systematic error.

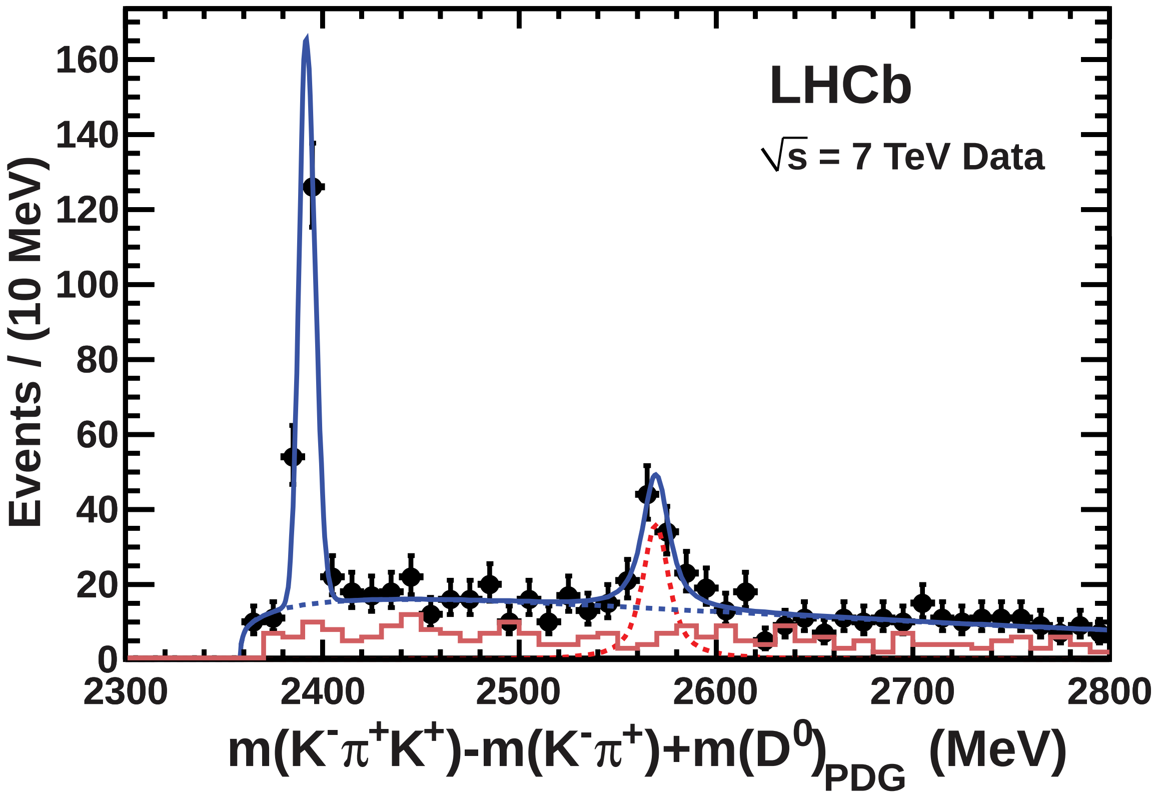

Figure 12: The mass difference $(K^-\pi^+K^+)$-$(K^-\pi^+)$ added to the known D^0 mass for events with $K^-\pi^+$ invariant masses within ± 20 MeV of the D^0 mass (black points) semileptonic decays in an in $\approx$20 pb^{-1} data sample. The solid line shows data with an additional K^- instead of a K^+ and thus are of wrong sign of charge to come from a single semileptonic decay. The resonant peaks are each fit to a signal relativistic Breit-Wigner and linear background.

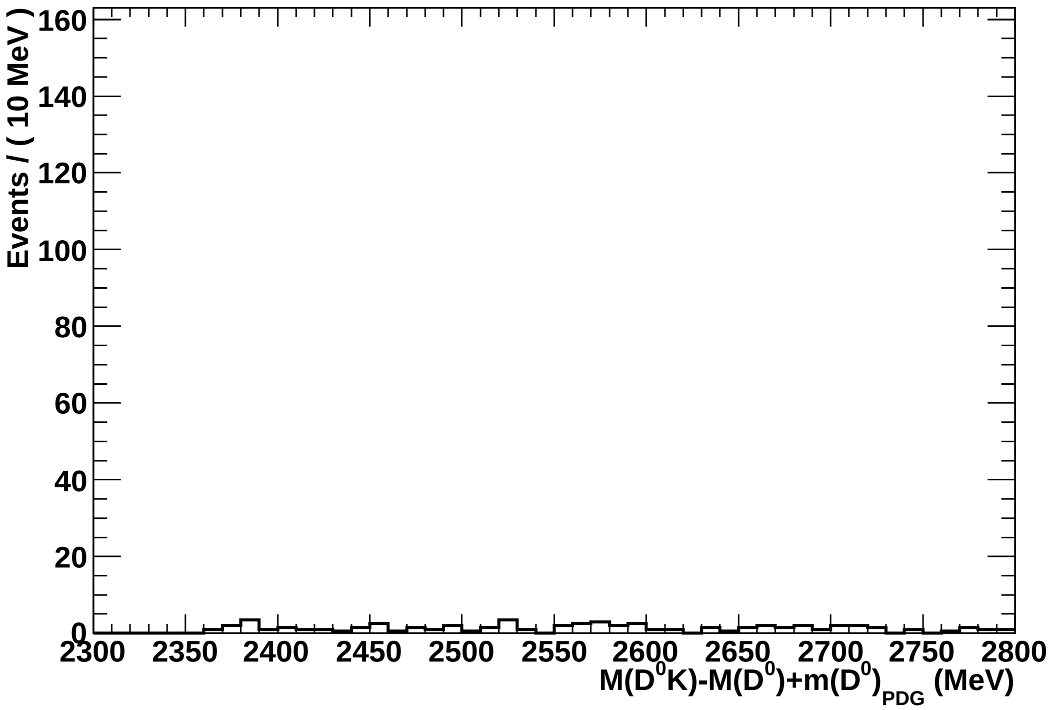

Figure 13: The mass difference $(K^-\pi^+K^+)$-$(K^-\pi^+)$ added to the known D^0 mass for events with $K^-\pi^+$ invariant masses in two sideband regions in the intervals 35-75 MeV away from the D^0 peak. The yield is scaled by a factor 0.5 to account for the ratio of the mass interval in signal and sidebands.

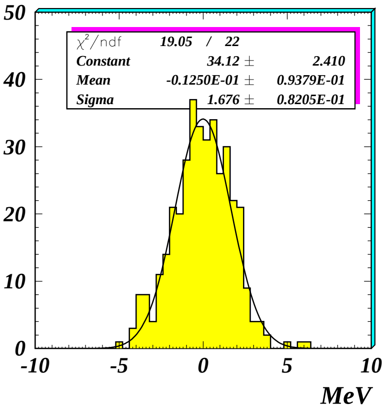

Figure 14: D_{s2}^{*+} mass derived from fits to an ensemble of toy MC using as an input the resonance parameters derived from the 20 pb^{-1} data.

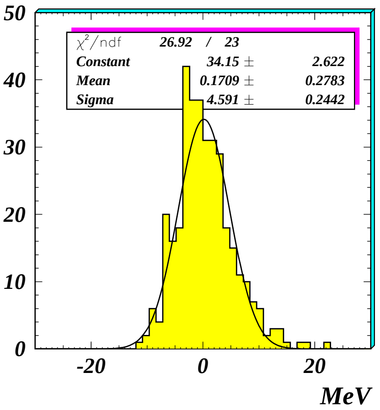

Figure 15: D_{s2}^{*+} width derived from fits to an ensemble of toy MC using as an input the resonance parameters derived from the 20 pb^{-1} data.

We use the 20 pb^{-1} sample for the measurement of the relative yields of D_{s1}^{+} and D_{s2}^{*+}. The fitted number of D_{s1}^{+} and D_{s2}^{*+} events are 155±15 and 82±17, respectively. We use this D_{s2}^{*+}/D_{s1}^{+} yield ratio, correcting for the lower detection efficiency for D_{s2}^{*+} of (0.516±0.017)%, compared with the D_{s1^+} efficiency of (0.598±0.025)% as

$$\frac{\mathcal{B}(\overline{B}_s^0 \to D_{s2}^{*+} X \mu^- \overline{\nu})}{\mathcal{B}(\overline{B}_s^0 \to D_{s1}^{+} X \mu^- \overline{\nu})} = 0.61 \pm 0.14 \pm 0.05. \tag{10}$$

The D_{s1}^{+} branching fraction relative to the $\overline{B}_s^0$ semileptonic rate is measured using the 3 pb^{-1} sample because the larger data set has a higher mean number of interactions per crossing, thus making it more difficult to determine the $\overline{B}_s^0$ semileptonic yield. This is ascertained by taking the total number of semileptonic $\overline{B}_s^0$ decays as the efficiency corrected sums of the $\overline{B}_s^0 \to D_s^+ X \mu^- \overline{\nu}$ and twice the $\overline{B}_s^0 \to D^0 K^+ \mu^- \overline{\nu}$ events. The systematic uncertainty on the $\overline{B}_s^0$ semileptonic yield is obtained from the systematic error on the D^0K^+ addition (6.3%), the $B \to D_s^+ K$ subtraction (2.0%) as listed in Table 6 and amounts to 6.6%.

We measure the branching fraction relative to the $\overline{B}_s^0$ semileptonic rate as

$$\frac{\mathcal{B}(\overline{B}_s^0 \to D_{s1}^{+} X \mu^- \overline{\nu})}{\mathcal{B}(\overline{B}_s^0 \to X \mu^- \overline{\nu})} = (5.5 \pm 1.2 \pm 0.5)\% \tag{11}$$

This branching fraction is obtained as follows. The number of $\overline{B}_s^0 \to D_{s1}^{+} \mu^- \overline{\nu} X$ is derived from the raw yield of 24.4 events by correcting for the $D^0 \to K\pi$ branching fraction (0.0389) and efficiency (0.598%). Finally, we multiply this number by 2 to account for the unseen isospin conjugate final state D^+K^0 and we get a yield of 2.1×10^5 events. The systematic error is dominated by uncertainties in the the $\overline{B}_s^0$ semileptonic yield which is 6.6%. More details on the extraction of the $\overline{B}_s^0$ semileptonic yield are given in Section VIII.

Our branching ratio for the D_{s1}^{+} is consistent with, but smaller than, the value of (9.8±3.0)% measured by D0 [13].

Finally, we use the measured ratio of branching fractions from Eq. 10 and the measured $\mathcal{B}(\overline{B}_s^0 \to D_{s1}^{+} X \mu^- \overline{\nu})$ to derive:

$$\frac{\mathcal{B}(\overline{B}_s^0 \to D_{s2}^{*+} X \mu^- \overline{\nu})}{\mathcal{B}(\overline{B}_s^0 \to X \mu^- \overline{\nu})} = (3.4 \pm 1.0 \pm 0.4)\%. \tag{12}$$

In addition to the components of the systematic error mentioned before, an additional 8% due to fitting the number of events in the peak is included for the $D_{s2^{*+}}$.

6 Background Studies

In order to evaluate the background contribution to the RS Dfb samples, we use generic $b\overline{b}$ Monte Carlo simulation. In the meson case, the background mainly comes from $b \to DDX$

with one of the $D's$ decaying semimuonically, and from combinations of tracks from the b and the $\bar{b}$ hadrons, where one decays into D and the other b decays semimuonically. The background subtractions are (1.9±0.3)% for $D^0 X\mu^-\overline{\nu}$, (2.5±0.6)% for $D^+ X\mu^-\overline{\nu}$, and (5.1±1.7)% for $D_s^+ X\mu^-\overline{\nu}$. The main background component for Λ_b semileptonic decays is $b\bar{b} \to \Lambda_b X$ with Λ_b decaying into $D_s\Lambda_c$, and the D_s decaying semimuonically. Overall, we find a background rate of 1.05±0.18 % RS events and 0.3±0.09% events. From this we infer a background fraction of (1.0±0.2)%.

7 Monte Carlo simulation and efficiency determination

We use dedicated Monte Carlo simulations, where b-hadron semileptonic decays are generated with HQET inspired form factor models described below. Particle identification efficiencies and trigger efficiency are determined from data.

The pion, kaon and proton efficiencies utilized in our simulation are determined using D^{*+}, Λ and K_s control samples where p, K, and π are selected without utilizing the particle identification criteria. The efficiency is obtained by simultaneously fitting the invariant mass distributions of events either passing or failing the identification requirements simultaneously. We illustrate the procedure adopted by giving the details on the proton identification extraction:

1. we apply HLT1& HLT2 TIS on proton,
2. we require the number of tracks to be less than 100,
3. we then fit the $p\pi$ invariant mass for events passing and for events failing the PID selection criteria simultaneously with the same double Gaussian signal shape, keeping the width floating, with the other parameters fixed to the values obtained from the integral fit over all p_t and η bin; while the background is modeled with a 2nd order polynomial whose parameters are allowed to float.
4. the total yield and PID efficiency are parameters in the fits

We have checked that the control sample used to derive the PID efficiency, and the data sample used for the b-fraction studies have similar multiplicities. They indeed are very similar but, contrary to our expectations, the minimum bias samples have a somewhat higher particle multiplicity. In order to correct for the relatively small difference, we divide both the signal and inclusive Λ samples into 5 subgroup of different multiplicities, and we reweigh the mass spectra by the ratio of mean relative population in the two samples. The fit results are used to derive matrices of π, K, p identification efficiencies as a function of the particle η and p_t. Fig. 16 shows the comparison between the track multiplicity in the sample used to derive the particle identification efficiency and the track multiplicity in the b-hadron sample. Fig. 17 shows the fits result for $p_t(p)$=(2.0,4.0) GeV. There are only a very few bins for which we cannot derive the efficiency from data due to lack of statistics, in this case we derive the efficiency from Monte Carlo, and we assign a 50% error to the estimate.

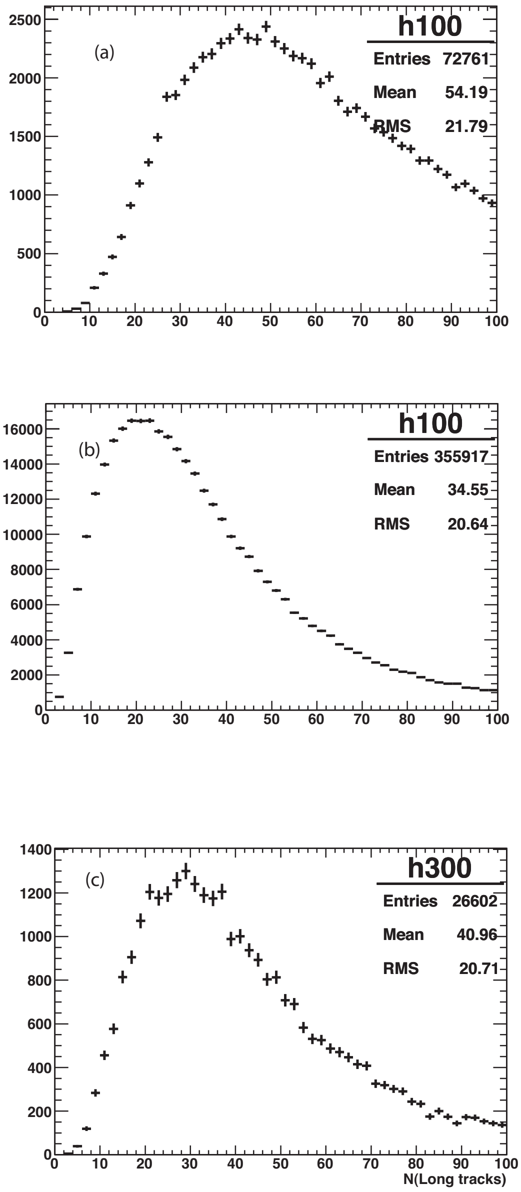

Figure 16: Multiplicity comparison between different samples used in this analysis: (a) the inclusive Λ used for the p identification efficiency estimate, (b) the K_s sample used for π identification efficiency determination, and (c) the $D^0\mu^-\overline{\nu}X$ sample.

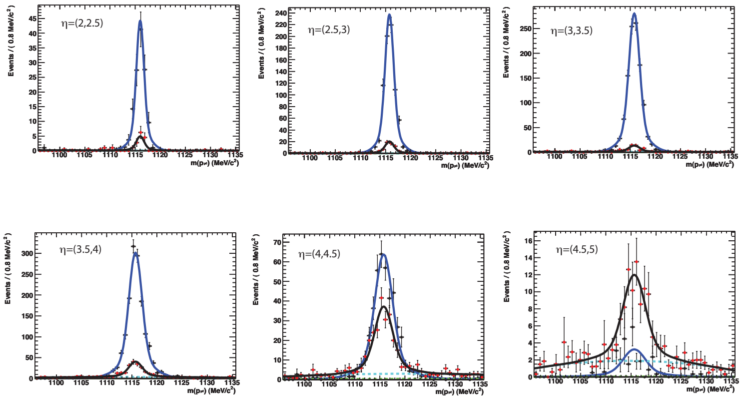

Figure 17: Examples of $\Lambda \to p\pi$ fits to determine the proton identification efficiency for $p_t(p) = (2, 4)$ GeV. The black dots correspond to the events passing the proton PID selection criteria, and the red dots correspond to events failing it.

Table 5: Efficiencies for particle identification as measured using our cuts and in our data sample. PT_L and PT_R refer to the lower and upper p_t range of the hadron, while η_L and η_R refer to the η lower and upper ranges.

PT_L (GeV)	PT_R (GeV)	η_L	η_R	Pion eff (%)	err (%)	Kaon eff (%)	err (%)	Proton eff(%)	err(%)
0.3	0.8	1.5	2.0	99.64	0.32	34.98	20.00	0.00	50.00
0.3	0.8	2.0	2.5	99.59	0.04	73.96	20.00	71.20	35.60
0.3	0.8	2.5	3.0	99.19	0.03	93.26	4.22	76.72	38.36
0.3	0.8	3.0	3.5	98.14	0.04	92.51	2.35	69.41	1.87
0.3	0.8	3.5	4.0	95.38	0.06	96.13	2.19	75.92	0.50
0.3	0.8	4.0	4.5	98.00	0.05	86.98	2.35	31.43	0.51
0.3	0.8	4.5	5.0	98.34	0.09	77.67	3.98	34.91	0.68
0.3	0.8	5.0	5.5	99.38	0.26	100.00	49.12	45.87	3.55
0.8	1.2	1.5	2.0	99.15	0.62	71.43	20.00	69.41	34.71
0.8	1.2	2.0	2.5	99.19	0.09	96.91	3.03	82.06	41.03
0.8	1.2	2.5	3.0	98.04	0.09	97.78	1.22	75.80	3.67
0.8	1.2	3.0	3.5	98.24	0.10	99.00	0.93	80.50	0.66
0.8	1.2	3.5	4.0	99.00	0.07	94.74	1.03	87.79	0.36
0.8	1.2	4.0	4.5	98.82	0.12	80.42	1.76	63.60	0.68
0.8	1.2	4.5	5.0	99.16	0.22	67.43	4.10	51.41	1.34
0.8	1.2	5.0	5.5	100.00	2.23	34.39	26.88	59.80	12.66
1.2	2.0	1.5	2.0	98.00	1.64	100.00	13.12	67.75	33.88
1.2	2.0	2.0	2.5	99.08	0.14	98.35	1.05	80.38	12.95
1.2	2.0	2.5	3.0	98.65	0.15	99.03	0.49	84.85	0.97
1.2	2.0	3.0	3.5	98.97	0.18	97.88	0.45	90.50	0.48
1.2	2.0	3.5	4.0	98.96	0.17	92.09	0.68	92.43	0.37
1.2	2.0	4.0	4.5	99.20	0.24	71.67	1.26	72.72	0.86
1.2	2.0	4.5	5.0	99.59	0.38	32.98	3.23	46.31	2.08
1.2	2.0	5.0	5.5	100.00	9.52	9.48	13.15	40.19	18.35
2.0	4.0	1.5	2.0	100.00	4.42	100.00	0.64	80.34	40.17
2.0	4.0	2.0	2.5	99.49	0.52	98.49	0.60	90.20	2.75
2.0	4.0	2.5	3.0	99.16	0.52	94.59	0.48	92.21	0.98
2.0	4.0	3.0	3.5	100.00	0.22	92.68	0.46	95.69	0.71
2.0	4.0	3.5	4.0	98.27	0.61	75.30	0.80	89.16	0.94
2.0	4.0	4.0	4.5	100.00	0.20	41.83	1.47	64.90	2.26
2.0	4.0	4.5	5.0	100.00	0.69	6.98	1.77	24.05	5.16
2.0	4.0	5.0	5.5	0.00	0.00	0.00	17.84	0.00	50.00
4.0	20.0	1.5	2.0	100.00	39.35	83.80	4.61	0.00	54.69
4.0	20.0	2.0	2.5	99.92	2.90	67.80	1.58	96.46	10.03
4.0	20.0	2.5	3.0	100.00	1.19	66.83	1.08	93.58	4.10
4.0	20.0	3.0	3.5	96.21	4.83	55.16	1.20	89.85	6.91
4.0	20.0	3.5	4.0	100.00	5.21	23.89	1.50	62.90	7.57
4.0	20.0	4.0	4.5	100.00	5.96	1.22	0.97	7.05	9.34
4.0	20.0	4.5	5.0	100.00	39.35	0.00	0.71	0.00	21.15
4.0	20.0	5.0	5.5	0.00	0.00	0.00	0.00	0.00	33.40

Fig. 18 shows the derived p efficiency as a function of the $\Lambda_c\mu$ p_t in the three η bins studied in this analysis.

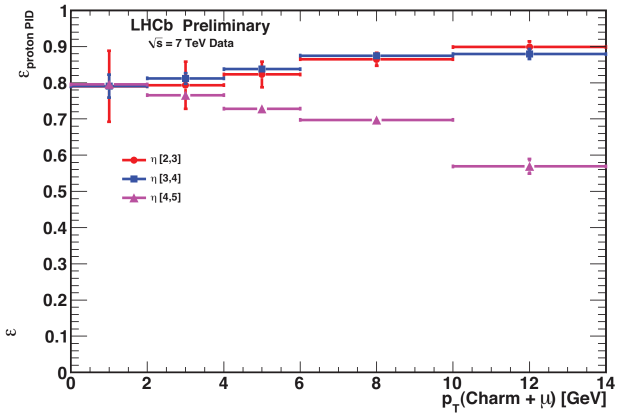

Figure 18: Measured proton identification efficiency as a function of the $\Lambda_c\mu$ p_t for $\eta = (2,3)$, $\eta = (3,4)$, $\eta = (4,5)$ respectively, and for the selection criteria used in the $\Lambda_c \to pK\pi$ mode.

We measure the HLT1 and HLT2 single muon efficiencies using TIS J/ψ from the lifetime biased dimuon stripping line.

The detection efficiency is determined from dedicated Monte Carlo samples of b-hadron semileptonic decays. The right choice of hadron spectrum and form factors affects the realism of the simulation. While much is known on the B^0 and B^+ semileptonic decays, the information on the corresponding $\overline{B}_s^0$ and Λ_b semileptonic decays is rather sparse.

The hadronic composition of the final states in $\overline{B}_s^0$ decays is poorly known [12]. The data sample used in this analysis can be exploited to gain insight into the hadron composition in the final state, utilizing a semi-exclusive method. We can infer the b hadron direction from the line of flight, connecting the nearest primary vertex to the hadron-μ secondary vertex. The b-hadron momentum p_B is determined up to a two-fold ambiguity due to the lack of knowledge of the orientation of the ν in the b-hadron rest frame with respect to its direction in the laboratory. We choose the lowest p_B solution. From the B hadron 4-vector, we can infer the ν 4-momentum, and thus calculate q^2 and perform 2 dimensional fits to the q^2 and $M_{\mu had}$ to determine the relative fraction of the exclusive final states considered. The data constrain the relative proportion of different final states, while theoretical models provide input on the form factor dependence of the hadronic current describing specific final states. In general, HQET has proven very successful in describing Cabibbo favored B meson semileptonic decays, and we assume that SU(3) is a reasonable assumption for these decays, as the mass of the s quark is reasonably smaller than the b quark mass.

In the case of the $\overline{B}_s^0 \to D_s$ semileptonic decays, we assume that they include D_s, D_s^*,

$D^*_{s0}(2317)$, $D_{s1}(2460)$, and $D_{s1}(2536)$ hadrons. Higher mass charm mesons decay predominantly to $D^{(*)}K$. We model the decays to the final states $D_s\mu^-\overline{\nu}$ and $D^*_s\mu^-\overline{\nu}$ with HQET form factors using normalization coefficients derived from studies of the corresponding $\bar{B}^0$ and B^- semileptonic decays [1], while we use the ISGW2 [14] form factor model to describe final states including higher mass resonances. We then perform a two-dimensional fit to the q^2-$M_{\mu D_s}$ distribution, and infer the D_s, D^*_s, and D^{**}_s fractions. Figure 19 shows the data compared with stacked histograms identifying the various components of the fit: D_s, D^*_s constrained to maintain the ratio $D^*_s/D_s = 2.42$, consistent with the weighted average of this ratio measured in $\overline{B}^0$ and B^- decays (2.42±0.10) [1]. The background shape and normalization is fixed, as it is derived from the combinatoric background under the D_s signal, so is the overall normalization, as we utilize all the signal events in the $D_s\mu^-\overline{\nu}X$ sample. Thus the ratio between the D^*_s and D_s hadrons in the final state is essentially the only free parameter in the fit. The fitting algorithm used is TFractionFitter, based on HMCMLL by Barlow and Beeston [15].

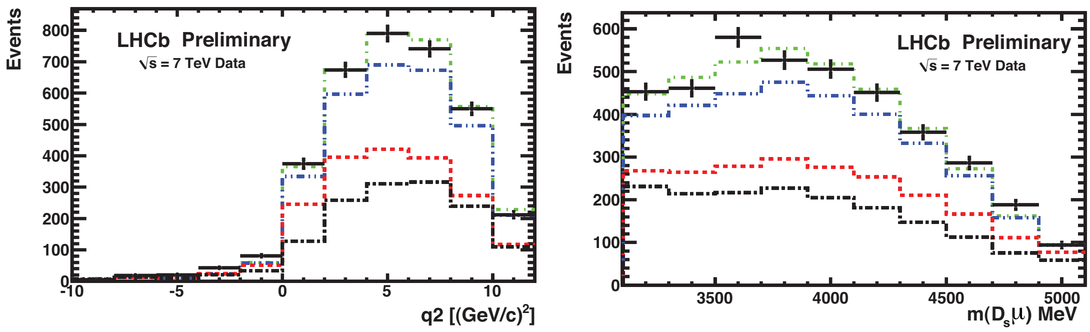

Figure 19: Projections of the two-dimensional fit to the q^2 and $M(D_s\mu)$ distributions of semileptonic decays including a D_s meson. The D^*_s/D_s ratio has been fixed to the measured D^*/D ratio in light B decays (2.42±0.10), and the background contribution is obtained using data fixed from the sidebands in the $K^+K^-\pi^+$ mass spectrum. The different components are stacked: the background is represented by a black dot-dashed line, D_s by a red dashed line, D^{*+}_s by a blue dash-double dotted line and D^{**}_s by a green dash-dotted line.

Similar considerations apply to Λ_b semileptonic decays. Only a study from CDF provides some constraints on the final states dominant in the corresponding Λ_b decays [16]. Also here we study q^2 and $M(\Lambda_c\mu)$ to gain some insight on the relative fractions of different hadron species in the final state. The results are shown in Fig. 20. In this case we consider three final states, $\Lambda_c\mu^-\overline{\nu}X$, $\Lambda_c(2595)\mu^-\overline{\nu}$, and $\Lambda_c(2625)\mu^-\overline{\nu}$, with form factors derived in the model of Ref. [22], and we constrain the two highest mass hadrons to be produced in the ratio predicted by theory. More details on these studies are given in Appendix C.

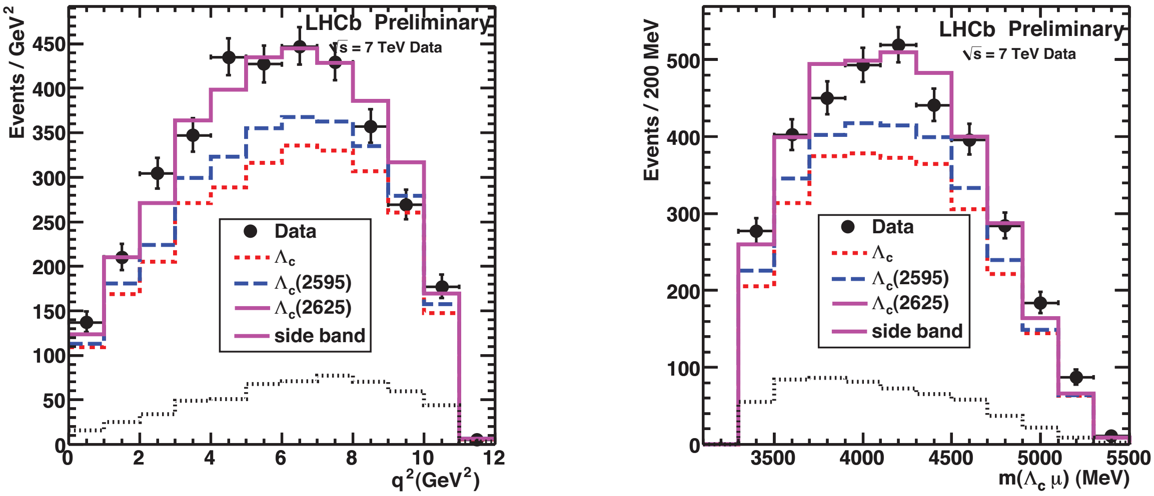

Figure 20: Fits to the q^2 distribution of semileptonic decays including a Λ_c meson. The different components are stacked.

8 Evaluation of $f_s/(f_u + f_d)$, and systematic checks

Perturbative QCD calculations lead us to expect the ratios $f_s/(f_u+f_d)$ and $f_{\Lambda_b}/(f_u+f_d)$ to be fairly independent of the pseudo-rapidity η, while a possible dependence upon the b-hadron transverse momentum p_t^b is not ruled out, especially for ratios involving baryon species [17]. Thus it interesting to study these ratios in different p_t^b intervals. For simplicity, we do not map the measured μ+hadron transverse momentum p_t into the primary b hadron distribution, but we simply split our sample into 5 p_t intervals. In addition, at low η, there is a low p_t interval where our acceptance is nearly zero. In order to determine the corrected yields entering the ratio $f_s/(f_u + f_d)$, we determine partial yields in a matrix of 3 η bins and 5 $p_t(\mu h)$ bins and divide them by the corresponding efficiencies.

Figs. 21, 22, 23 show the ln(IP/mm) fits for the $D^0\mu^-\overline{\nu}X$ channel, in the three η interval studied. They illustrate the quality of the fits for this channel.

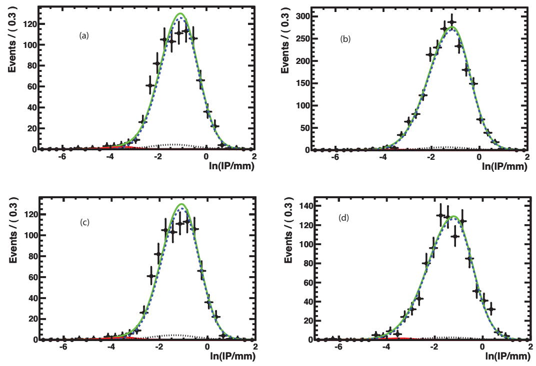

Figure 21: Logarithm of (IP/mm) fits for (a) p_t=(2,4), (b) p_t=(6,8), (c) p_t=(8,10), (d) p_t=(10,14) in the η=(2,3) interval for $D^0\mu^-\overline{\nu}X$.

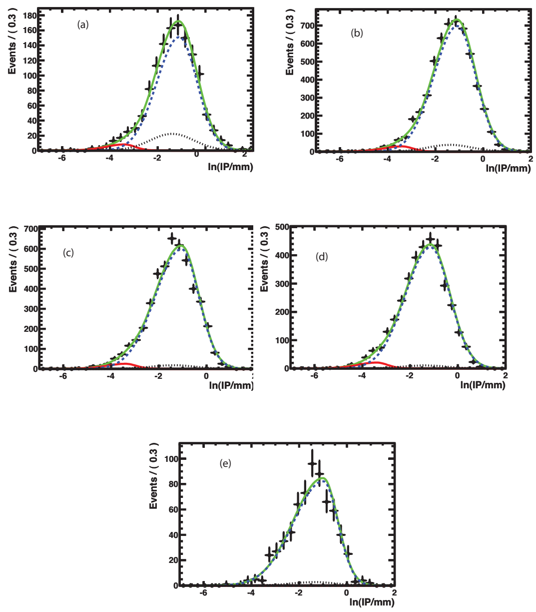

Figure 22: Logarithm of (IP/mm) fits for (a) p_t=(0,2), (a) p_t=(2,4), (b) p_t=(6,8), (c) p_t=(8,10), (d) p_t=(10,14) in the η=(3,4) interval for $D^0\mu^-\overline{\nu}X$.

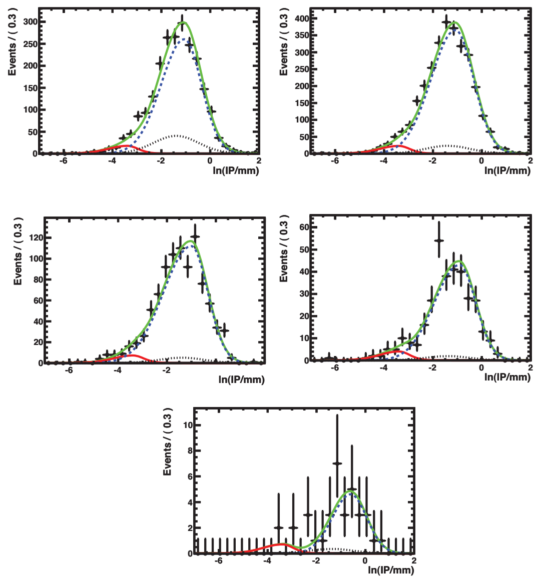

Figure 23: Logarithm of (IP/mm) fits for (a) p_t=(0,2), (a) p_t=(2,4), (b) p_t=(6,8), (c) p_t=(8,10), (d) p_t=(10,14) in the η=(4,5) interval for $D^0\mu^-\overline{\nu}X$.

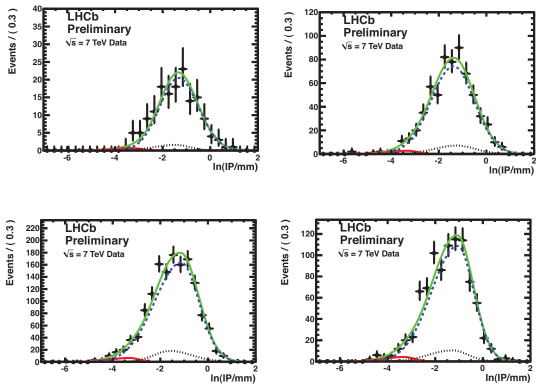

Figure 24: Logarithm of (IP/mm) fits for (a) p_t=(2,4), (b) p_t=(6,8), (c) p_t=(8,10), (d) p_t=(10,14) in the η=(2,3) interval for $D^+\mu^-\overline{\nu}X$.

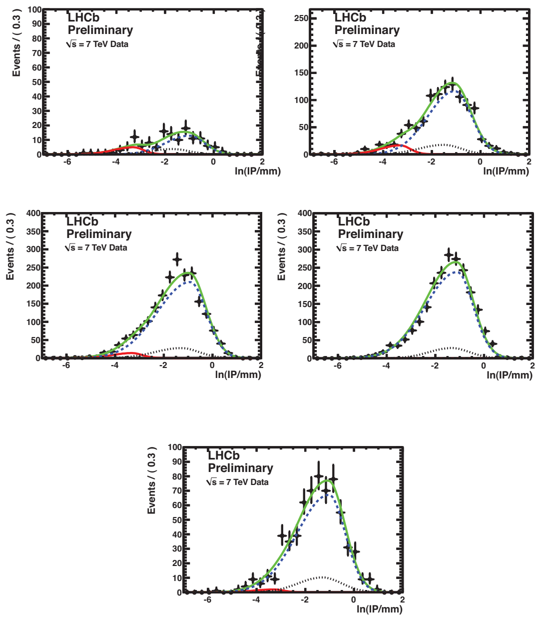

Figure 25: Logarithm of (IP/mm) fits for (a) p_t=(0,2), (a) p_t=(2,4), (b) p_t=(6,8), (c) p_t=(8,10), (d) p_t=(10,14) in the η=(3,4) interval for $D^+\mu^-\overline{\nu}X$.

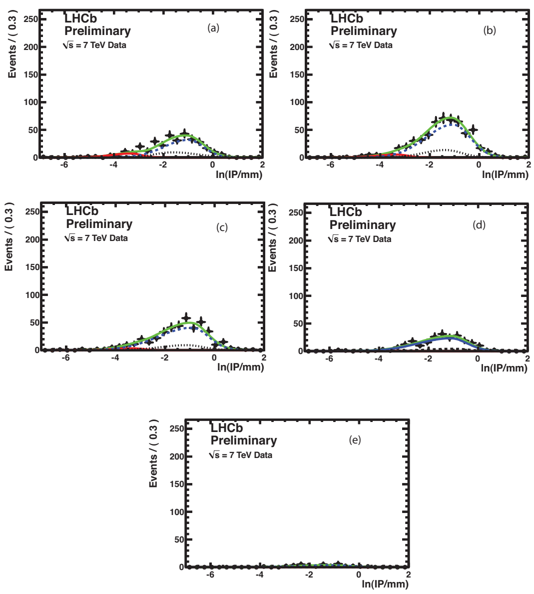

Figure 26: Logarithm of (IP/mm) fits for (a) p_t=(0,2), (a) p_t=(2,4), (b) p_t=(6,8), (c) p_t=(8,10), (d) p_t=(10,14) in the η=(4,5) interval for $D^+\mu^-\overline{\nu}X$.

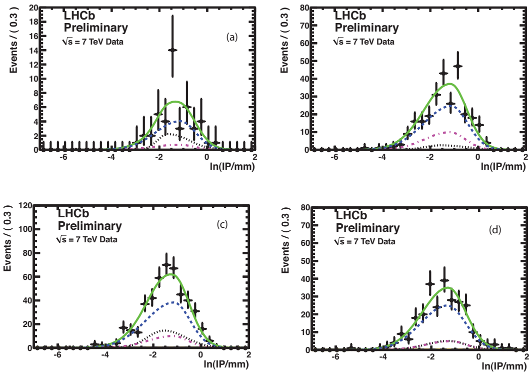

Figure 27: Logarithm of (IP/mm) fits for (a) p_t=(2,4), (b) p_t=(6,8), (c) p_t=(8,10), (d) p_t=(10,14) in the η=(2,3) interval for $D_s\mu^-\overline{\nu}X$.

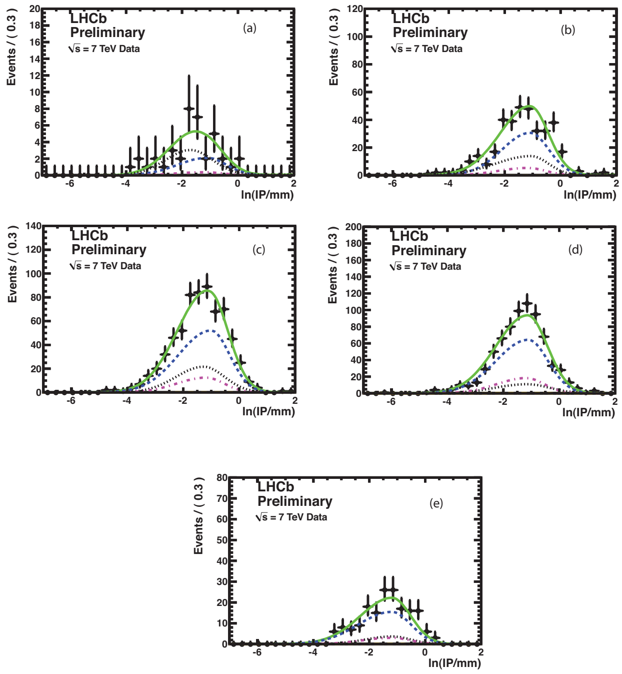

Figure 28: Logarithm of (IP/mm) fits for (a) p_t=(0,2), (a) p_t=(2,4), (b) p_t=(6,8), (c) p_t=(8,10), (d) p_t=(10,14) in the η=(3,4) interval for $D_s\mu^-\overline{\nu}X$.

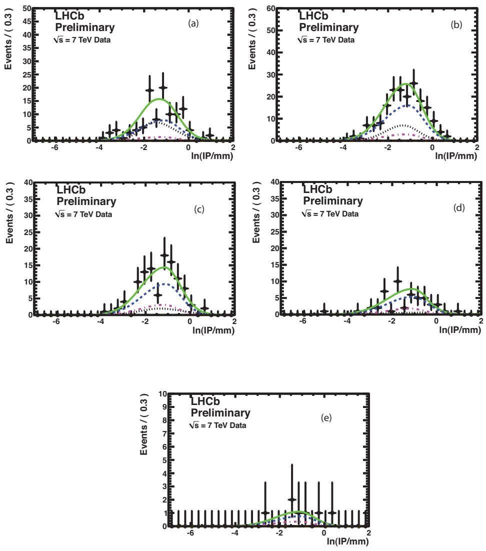

Figure 29: Logarithm of (IP/mm) fits for (a) p_t=(0,2), (a) p_t=(2,4), (b) p_t=(6,8), (c) p_t=(8,10), (d) p_t=(10,14) in the η=(4,5) interval for $D_s\mu^-\overline{\nu}X$.

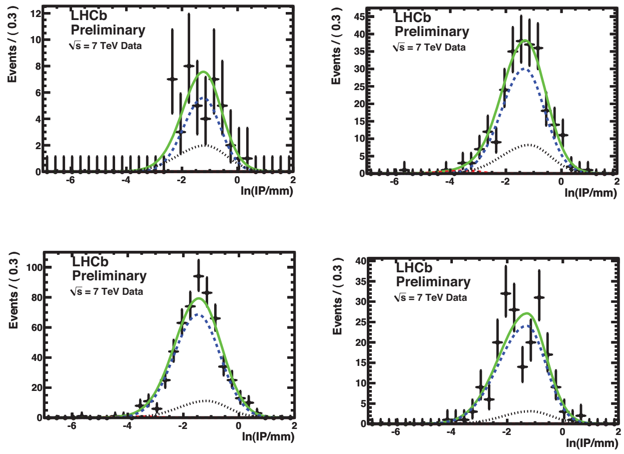

Figure 30: Logarithm of (IP/mm) fits for (a) p_t=(2,4), (b) p_t=(6,8), (c) p_t=(8,10), (d) p_t=(10,14) in the η=(2,3) interval for $\Lambda_c \mu^- \overline{\nu} X$.

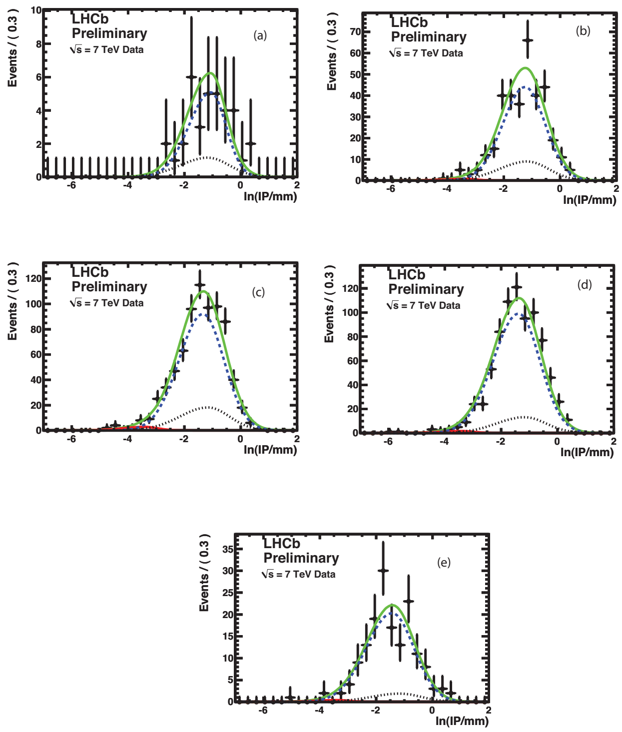

Figure 31: Logarithm of (IP/mm) fits for (a) p_t=(0,2), (b) p_t=(2,4), (c) p_t=(6,8), (d) p_t=(8,10), (e) p_t=(10,14) in the η=(3,4) interval for $\Lambda_c \mu^- \overline{\nu} X$.

We have studied the MC samples in the same manner, determining the efficiency in each $\eta - p_t$ rectangular domain. Fig. 33 shows the simulation results.

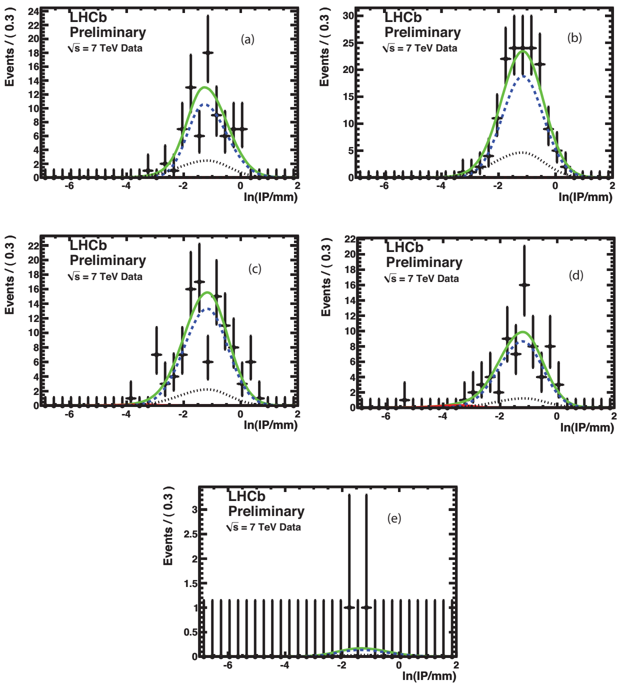

Figure 32: Logarithm of (IP/mm) fits for (a) p_t=(0,2), (a) p_t=(2,4), (b) p_t=(6,8), (c) p_t=(8,10), (d) p_t=(10,14) in the η=(4,5) interval for $\Lambda_c\mu^-\overline{\nu}X$.

In order to understand the shapes of the efficiency curves shown here, we have examined the efficiency trends in three steps:

1. first we check that final state studied is within the LHCb acceptance, and that the tracks are reconstructed as "long tracks;"

2. then we apply the muon trigger, muon PID, and we all the p_T cuts described in the analysis procedure description,

4. lastly, we apply the particle identification criteria.

Fig. 34 shows the results obtained for the $D^0\mu$ final state. It can be seen that the efficiency loss at low p_t is driven largely by the p_t cuts, and that the efficiency is reasonably constant after it reaches its asymptotic value. Figs. 35, 36, 37 show the corresponding analysis for the $(D^+D_s\Lambda_c)\mu^-\overline{\nu}X$ final states.

There are two efficiency ratios that are necessary to complete the evaluation of $f_s/(f_u+f_d)$. We need $\epsilon(\overline{B}_s^0 \to D^0K)/\epsilon(\overline{B}_s^0 \to D^0)$, and $\epsilon(\overline{B} \to D_s)/\epsilon(Bs \to D_s)$. The former is evaluated with the MC samples used for the D^0K analysis, and is 0.232±0.006. The latter required some care, because of the absence of a proper modeling of the decay $B^+ \to D_s^{(*)}K\mu^-\overline{\nu}$. Thus we first simulate the decay of $B \to D_sK\mu^-\overline{\nu}$ with a phase space generator, then re-weight in bins of p_μ^{*B} at the generator level to match the distribution of the Goity Roberts model for the decay generated $B \to D\pi\mu\nu$, to obtain the right μ spectrum arising from the semileptonic decay $b \to c\mu\nu$. After re-weighting we get $\epsilon(|overline(B) \to D_s) = (0.73 \pm 0.03)\%$. The corrections to $n_{\rm corr}(D^0X\mu^-\overline{\nu})$ from $D^0K^+X\mu^-\overline{\nu}$ and $D^0pX\mu^-\overline{\nu}$ amount to a 1.8% subtraction. For $D^+X\mu^-\overline{\nu}$ the subtraction is 3.7%. These corrections are applied uniformly in all η and p_t bins. We do not subtract muon fakes, about a 0.5% effect, or $b \to D\tau^+X\overline{\nu}$ backgrounds, about a 1.5% effect, as these are taken to be the same for all the b species.

Once we determine the corrected yields in our matrix of p_t-η domains, Eq. **??** gives the desired fractions, using the lifetime ratio $(\tau_{B^-} + \tau_{\overline{B}^0})/2\tau_{\overline{B}^0_s} = 1.07 \pm 0.02$. The measured ratio is fairly constant over the whole η-p_t domain.

By fitting the data to a constant, we obtain $f_s/(f_u + f_d) = 0.132 \pm 0.006 \pm 0.002$ in $\eta = (2,3)$ and $0.135 \pm 0.004 \pm 0.002$ in $\eta = (3,5)$, where the first errors are statistical and the second reflect systematic uncertainties due to MC statistics and K identification efficiency determination. The fits are shown in Fig. 38. Finally, by fitting all the 14 data points to a single constant, we determine $f_s/(f_u + f_d) = 0.134 \pm 0.004 \pm 0.001$, where the last error accounts only for MC statistics and K identification efficiency errors. In evaluating the systematic errors we have taken into account the correlations between different η and p_t bins introduced in the particle identification efficiency error. From this we have derived an error matrix with off diagonal elements derived from overlap in p_t and η between K that form D_s candidates populating different $\overline{B}^0_s$ p_t and η bins. The detection efficiency and particle identification efficiency systematic errors are evaluated bin by bin. The errors induced by uncertainties in the K identification efficiency have been calculated by estimating the full error matrix associated with it. We have evaluated it by constructing a 14x40 weight matrix W_{ij} giving the fraction of K population from a given η and p_t bin, and then construct the covariance matrix WAW^T, where A is a diagonal 40x40 K identification efficiency covariance matrix derived from the errors shown in Table 5. We have checked with toy Monte Carlo simulations that the other particle identification efficiency uncertainties are negligible, as they are very small (π in D^+), or largely cancel in the ratio (K and π in D^0, D_s, and D^+). In this algorithm, we calculate the relevant corrected partial yields with the efficiency defined as the product of a trigger-reconstruction efficiency and the relevant particle identification efficiencies. For example for D^0, we define the efficiency in each bin as

$$\epsilon_i = \epsilon_i^r \times \epsilon_i^K \epsilon_i^\pi \tag{13}$$

and we derive the PID efficiencies from Table 5 as

$$\epsilon_i^K = \Sigma_j W_{ij}^{D^0 \to K} \times \epsilon_j(K), \tag{14}$$

and

$$\epsilon_i^\pi = \Sigma_j W_{ij}^{D^0 \to \pi} \times \epsilon_j(\pi), \tag{15}$$

where W_{ij} represent the fractions of particles with p_T and η in bin j for the $D_s\mu$ p_t and η within the domain corresponding to the index i. We then vary the parameters $\epsilon_j(K)$, and $\epsilon_j(\pi)$ with Gaussian probability distributions and we examine the variation of $f_s/(f_u+f_d)$. In each bin these variations are negligible compared with the errors considered. We have applied the same procedure in taking account the errors associated with each bin and their correlations, in the evaluation of f_+/f_0 and $f_{\Lambda_b}/(f_u + f_d)$.

Table 6: Systematic errors on the relative $\overline{B}^0_s$ production fraction.

Source	Error (%)
Bin dependent errors	1.0
Charm hadron branching fractions	5.5
B_s semileptonic decay modeling	3.0
Backgrounds	2.0
Tracking efficiency	2.0
Lifetime ratio	1.8
PID efficiency	1.5
$\overline{B}^0_s \to D^0 K^+ X \mu^- \overline{\nu}$	${}^{+4.1}_{-1.1}$
$(B^-, \overline{B}^0) \to D_s^+ K X \mu^- \overline{\nu}$	2.0
Total	${}^{+8.6}_{-7.7}$

In addition to the Monte Carlo statistical error and K identification efficiency error, which vary across the p_T-η domains studied, there are global multiplicative errors that affect $f_s/(f_u+f_d)$; they are listed in in Table 6. The dominant component is caused by the branching ratio error on $\mathcal{B}(D_s^+ \to K^+K^-\pi^+)$ of 4.9%. We use this decay mode rather than a combination of the resonant $\phi\pi^+$ and $K^{*0}K^+$ contributions, because these D_s decays do not have well defined branching fractions due to interferences in the Dalitz plot. Adding in the contributions of the D^0 and D^+ branching fractions we have a systematic error of 5.5% just due to the charm hadron branching fractions. Most systematic errors due to backgrounds, muon fakes etc. cancel in the ratio. The tracking efficiency errors mostly cancel in the ratio since we are dealing only with combinations of 3 or 4 tracks. The lifetime ratio error reflects the present experimental accuracy[1]. The PID efficiency error accounts for the sensitivity to the event multiplicity, and has been derived by comparing the K identification efficiency without correcting for different track multiplicity in the calibration and signal sample with the one obtained by reweighing mass spectra to account for these differences. The error on the $\overline{B}^0_s \to D^0 K^+ X \mu^- \overline{\nu}$ is obtained by changing the MC predicted RS/WS background ratio within errors, and evaluating the corresponding change in $[f_s/(f_u+f_d)]$. Finally, the error on $B^-\overline{B}^0 \to D_s^+ K X \mu^- \overline{\nu}$ reflects the uncertainty in the measured branching fraction. By adding these errors in quadrature with the bin dependent systematic error we obtain

$$\frac{f_s}{f_u + f_d} = 0.134 \pm 0.004^{+0.011}_{-0.010}. \tag{16}$$

Finally, we can examine the η dependence of $f_s/(f_u + f_d)$.Table 7 summarizes its determination as a weighted average of the individual data points, and through the fit procedure described before. The results obtained with both approaches are consistent, and show that there is no evidence for an η dependence of this fraction.

Table 7: η dependence of $f_s/(f_u + f_d)$ Only the statistical errors are shown.

η	$f_s/(f_u + f_d)$ (fit)	$f_s/(f_u + f_d)$ (average)
(2,3)	0.132±0.006	0.132±0.006
(3,4)	0.133±0.005	0.133±0.005
(4,5)	0.145±0.011	0.145±0.011

Assuming that $f_d = f_u$ we can compare $f_+/f_0 \equiv n_{\rm corr}(D^+)/n_{\rm corr}(D^0)$ with its expected value. It is not possible to decouple the two ratios for an independent determination of f_u/f_d. Using all the known semileptonic branching fractions [1], we estimate the relative fraction of the D^+ and D^0 modes from $B^{+/0}$ decays to be $f_+/f_0 = 0.375 \pm 0.023$, where the error includes a 6% theoretical uncertainty. Our corrected yields correspond to $f_+/f_0 = 0.373 \pm 0.006$ (stat) $\pm$ 0.007 (eff) $\pm$ 0.014, for a total uncertainty of 4.5%. The last error accounts for uncertainties in B background modeling, in $D^0 K^+ \mu^- \overline{\nu}$ yield, in the $D^0 p \mu^- \overline{\nu}$ yield, the D^0 and D^+ branching fractions, and the residual tracking efficiency uncertainties. The other systematics mostly cancel in the ratio. Our measurement is in agreement with the expectation.

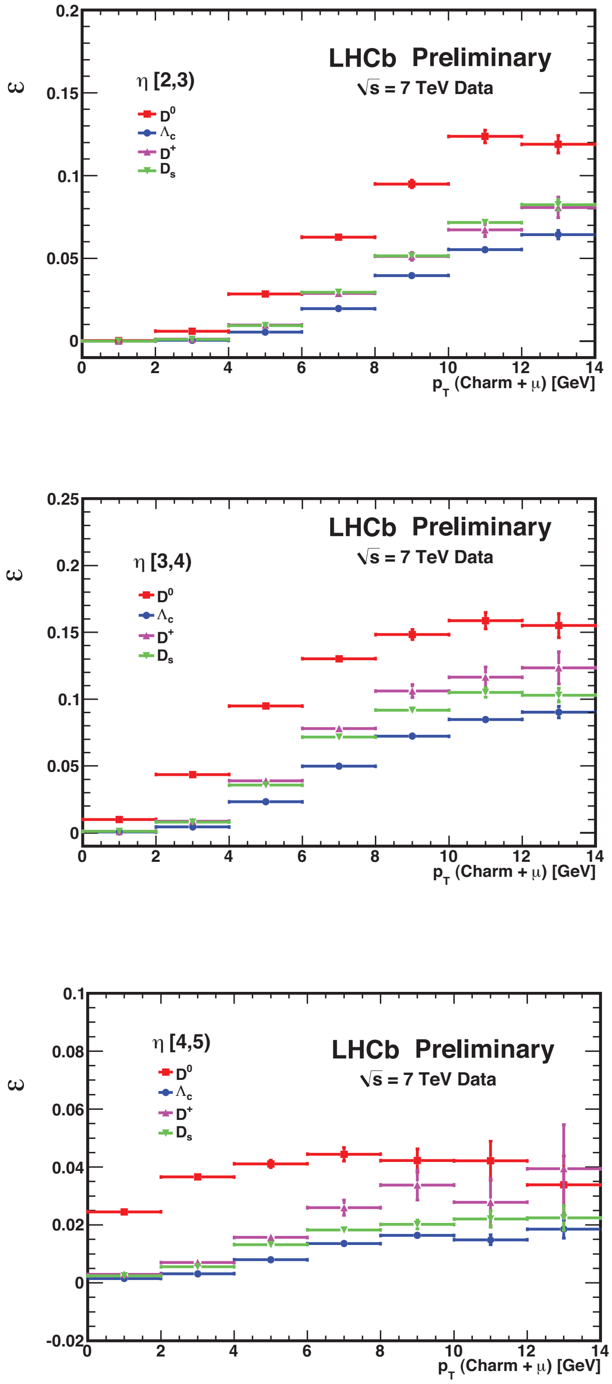

Figure 33: Efficiencies for $D^0\mu^-\overline{\nu}X$, $D^+\mu^-\overline{\nu}X$, $D_s\mu^-\overline{\nu}X$, $\Lambda_c\mu^-\overline{\nu}X$ as a function of η and p_t.

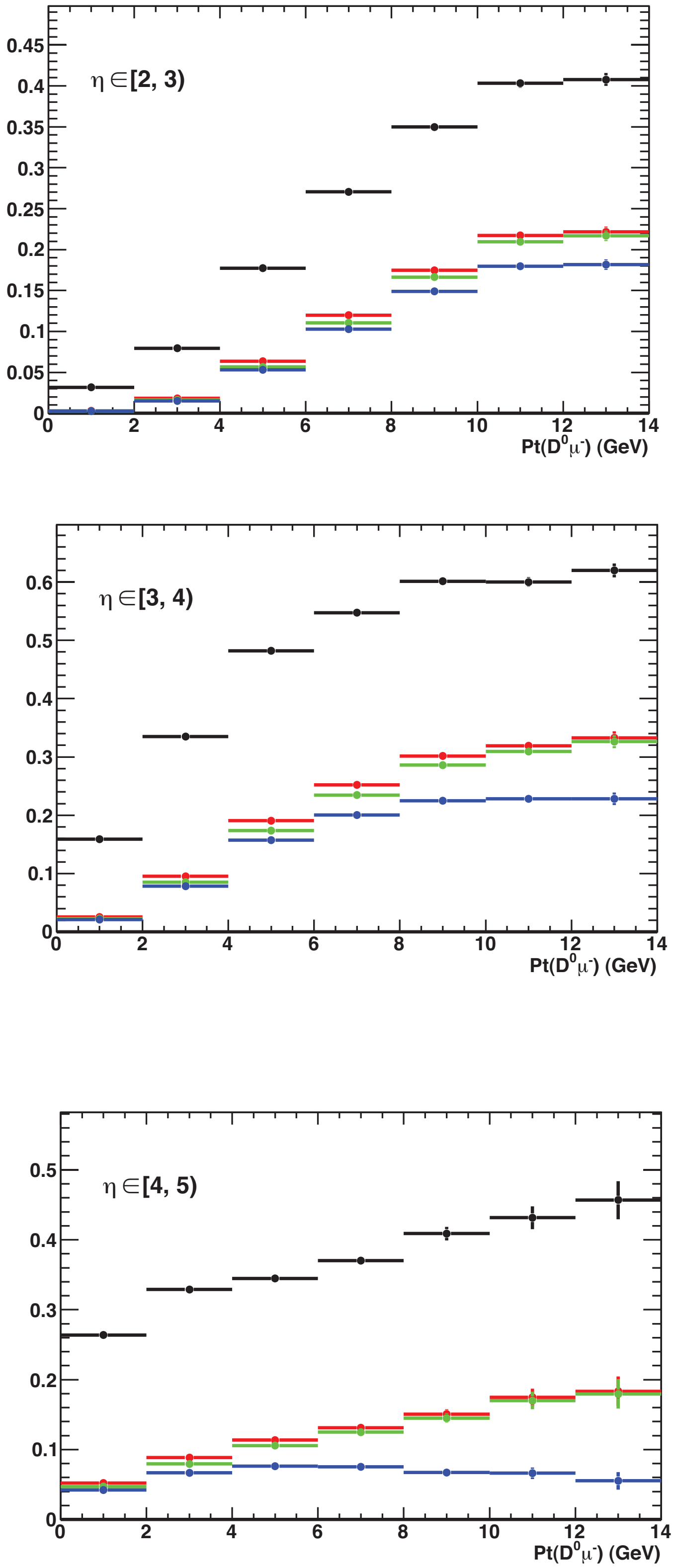

Figure 34: Efficiencies for $D^0\mu^-\overline{\nu}X$ upon applying sequentially: a) reconstruction and tracking criteria, b) muon trigger, identification and p_T cuts, c) K and π p_T cuts, d) K and π PID cuts for $4 \leq \eta \leq 5$.

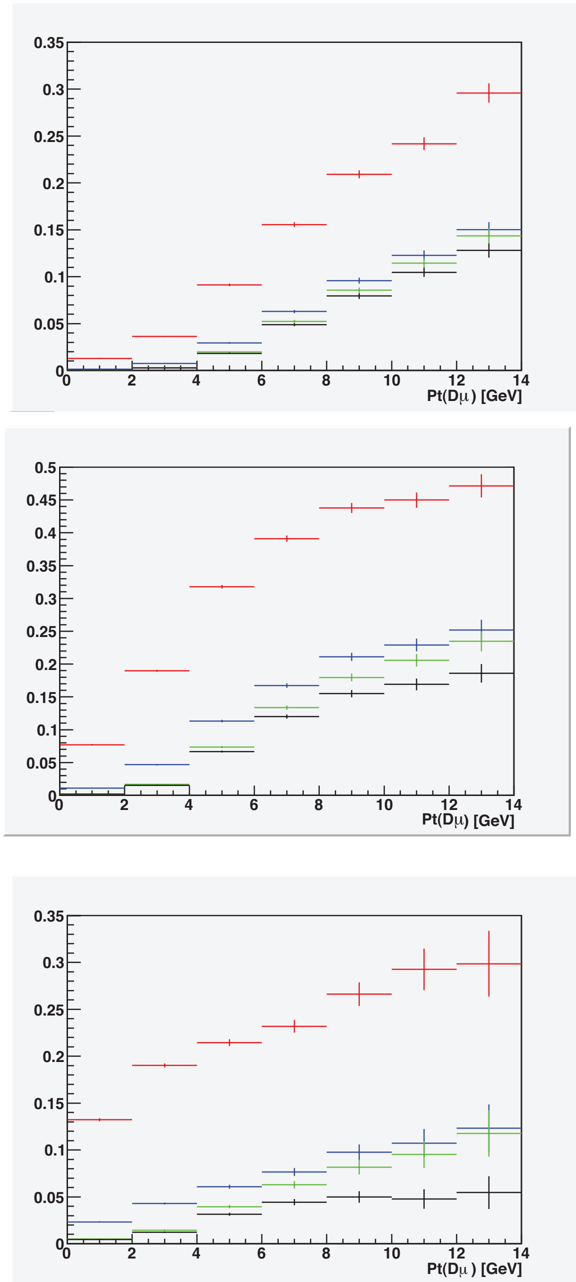

Figure 35: Efficiencies for $D^{+}\mu^{-}\overline{\nu}X$ upon applying sequentially: a) reconstruction and tracking criteria, b) muon trigger, identification and p_T cuts, c) K and π p_T cuts, d) K and π PID cuts for $4 \leq \eta \leq 5$.

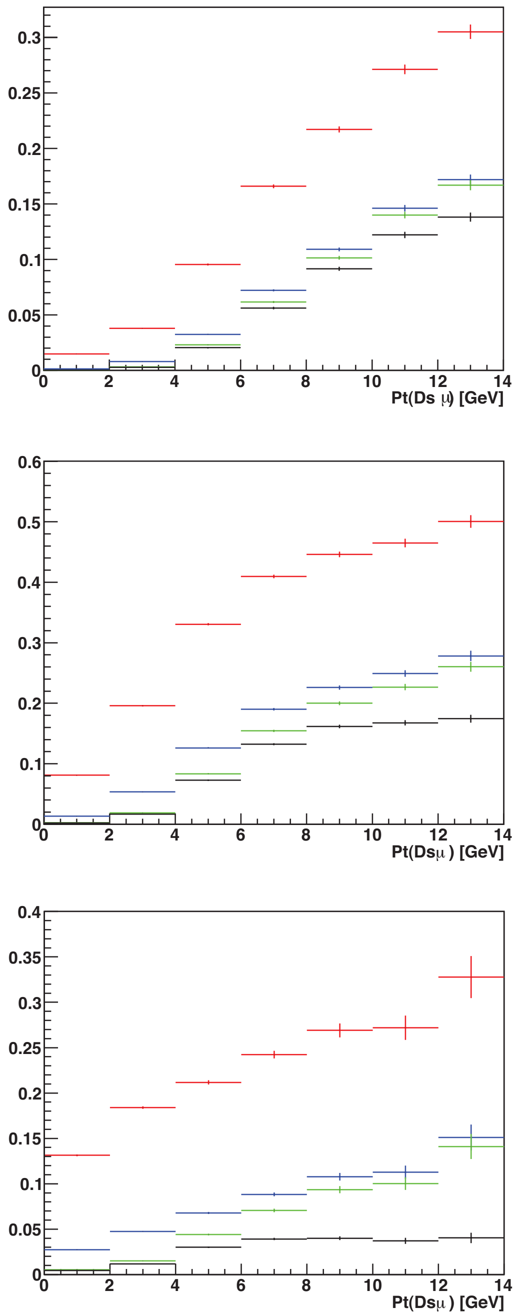

Figure 36: Efficiencies for $D_s\mu^-\overline{\nu}X$ upon applying sequentially: a) reconstruction and tracking criteria, b) muon trigger, identification and p_T cuts, c) K and π p_T cuts, d) K and π PID cuts for $4 \leq \eta \leq 5$.

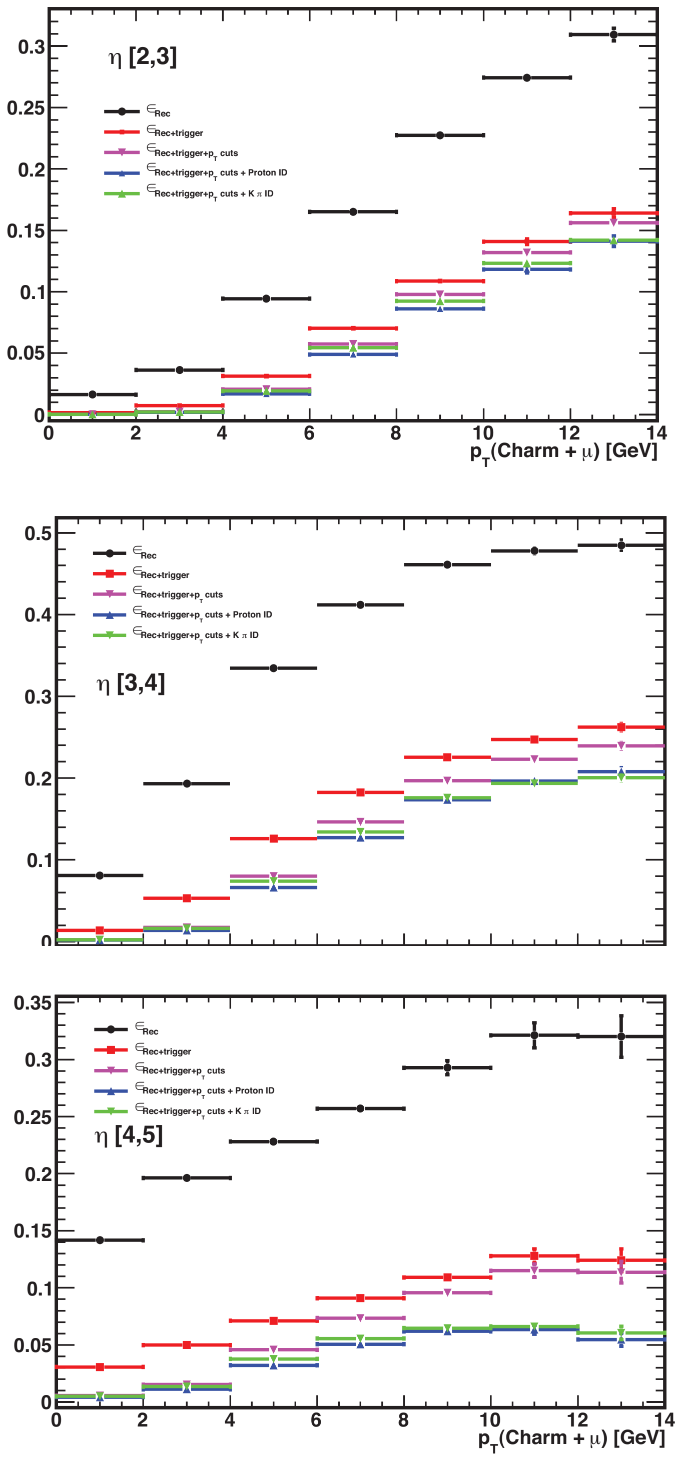

Figure 37: Efficiencies for $\Lambda_c\mu^-\overline{\nu}X$ upon applying sequentially: a) reconstruction and tracking criteria, b) muon trigger, identification and p_T cuts, c) K and π p_T cuts, d) K and π PID cuts for $4 \leq \eta \leq 5$.

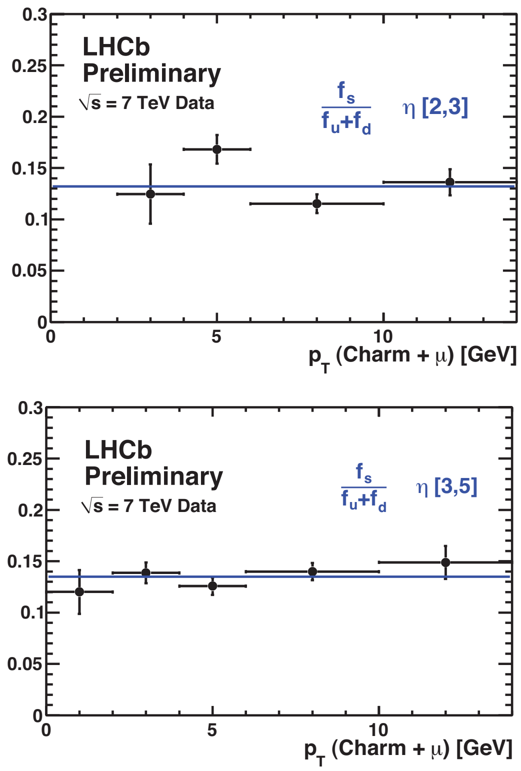

Figure 38: Ratio between $\overline{B}_s^0$ and light B meson productions as a function of the transverse momentum of the $D_s\mu$ pair. The errors shown are statistical only.

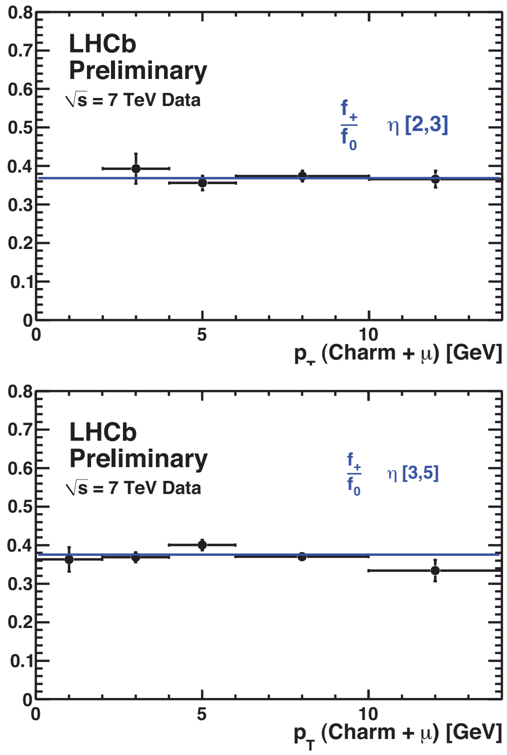

Figure 39: $\frac{f_+}{f_0}$ as a function of p_t for η=(2,3) (a) and η=(3,5) (b). The horizontal line shows the average value. The error shown combine the statistical errors and the systematic errors accounting for the detection efficiency and the particle identification efficiency.

9 Evaluation of $f_{\Lambda_b}/(f_u + f_d)$

We use Eq. 5 to compute the ratio of Λ_b production to light B meson production, and we determine the raw yields in the same grid of η-p_t domains used to evaluate $f_s/(f_u + f_d)$. We then correct the background subtracted raw yields for efficiency and the $\Lambda_c \to pK\pi$ branching fraction (5.0±1.3)% [1]. Then we add the contribution from $\Lambda_b \to D^0 p\mu^- \overline{\nu} X$. The average efficiency correction of (0.67±0.02)% is derived from MC simulation. In this case, we observe a linear dependence upon p_t of the $\Lambda_c\mu$ pair in all the η intervals. Fig. 40 shows our results. In this case we fit the data to a straight line

$$\frac{f_{\Lambda_b}}{f_u + f_d} = a[1 + b \times p_t(\mathrm{GeV})] \tag{17}$$

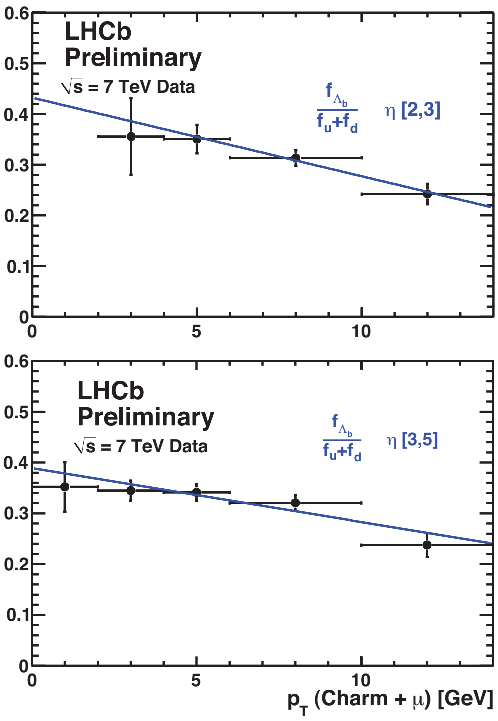

Figure 40: Fragmentation ratio $f_{\Lambda_b}/(f_u+f_d)$ dependence upon $p_t(\mu\Lambda_c)$. The errors shown are statistical only.

Table 8 summarizes the fit results. The linear fit is used to quantify the hypothesis that the fraction $f_{\Lambda_b}/(f_u + f_d)$ is dependent upon the p_t of the $\Lambda_c\mu$ pair. We have also fitted the data points to a constant, in this case we obtain $f_{\Lambda_b}/(f_u + f_d) = 0.290 \pm 0.013$ for $\eta = (2, 3)$ and $f_{\Lambda_b}/(f_u + f_d) = 0.321 \pm 0.009$ for $\eta = (3, 5)$. Table 10 summarizes the confidence level for the various fits that we have attempted, and corresponding exclusion limit in terms of number of sigmas. A fraction constant with p_t ise excluded at 4 σ level.

Table 8: Coefficients of the linear fit describing the $p_t(\mu\Lambda_c)$ dependence of $f_{\Lambda_b}/(f_u + f_d)$. The systematic errors included are only those associated with the bin-dependent MC and particle identification errors .

η range	a	b
2-3	0.434±0.040±0.025	-0.036±0.008±0.004
3-5	0.397±0.020±0.009	-0.028±0.006±0.003
2-5	0.404±0.017±0.009	-0.031±0.004±0.003

Table 9: Systematic uncertainties on the absolute scale of $f_{\Lambda_b}/(f_u + f_d)$.

Source	Error (%)
Bin dependent errors	2.2
$\Lambda_b \to D^0 pX\mu^-\overline{\nu}$	2.0
Monte Carlo modeling	1.0
Backgrounds	3.0
Tracking efficiency	2.0
Γ_{sl}	2.0
Lifetime ratio	2.6
PID efficiency	2.5
Total Experimental	6.3
$\mathcal{B}(\Lambda_c \to pK\pi)$	26.0
Total	26.8

In order to quantify the p_t dependence of $[f_{\Lambda_b}/(f_u + fd)$, we have performed also fits to a single constant, in different η intervals. Fits to a constant give $[f_{\Lambda_b}/(f_u + f_d)] = 0.290 \pm 0.011 \pm 0.005$ for $\eta = (2, 3)$ and $[f_{\Lambda_b}/(f_u + f_d)] = 0.321 \pm 0.008 \pm 0.003$ for $\eta = (3, 5)$, where the quoted errors are statistical and bin dependent systematic error, due to MC statistic and proton identification efficiency i. Similarly, by splitting the latter interval into two η bins, we get $[f_{\Lambda_b}/(f_u + f_d)] = 0.330 \pm 0.009 \pm 0.004$ for $3 \leq \eta < 4$ and

Table 10: Fit quality of different fits tried

Method	χ^2	N(dof)	C.L.	exclusion (# of σs)
constant (2 η bins)	41.8	12	3.6×10^{-5}	4
constant (3 η bins)	37.7	11	8.8×10^{-5}	3.8
linear (2 η bins)	19.0	10	4×10^{-2}	2.6
linear (3 η bins)	7.2	8	0.52	0.1

$[f_{\Lambda_b}/(f_u + f_d)] = 0.284 \pm 0.020 \pm 0.006$ for $4 \leq \eta \leq 5$.

In view of the observed dependence upon p_t, we quote $[f_{\Lambda_b}/(f_u+f_d)] = (0.404 \pm 0.017 \pm 0.027 \pm 0.105) \times [1-(0.031 \pm 0.004 \pm 0.003) \times p_t(\text{GeV})]$, where the multiplicative errors are statistical, experimental, and absolute scale uncertainty due to the error in $\mathcal{B}(\Lambda_c \to pK\pi)$. Previous measurements of this fraction have been made at the LEP and the Tevatron[18]. LEP obtains 0.113±0.020. CDF measures $f_{\Lambda_b}/(f_u + f_d) = 0.281 \pm 0.012^{+0.011+0.128}_{-0.056-0.086}$, where the last error reflects the uncertainty in $\mathcal{B}(\Lambda_c \to pK\pi)$. The CDF paper [18] suggests that the difference between the Tevatron and LEP results is explained by the different kinematics of the two experiments, most notably the different mean p_T of the b quark, and, consequently, of the hadron-μ pair. It is interesting to note that LHCb probes an even lower b p_T range, while retaining some sensitivity in the CDF kinematic region. In view of the linear dependence upon p_t, we quote $[f_{\Lambda_b}/(f_u + f_d)] = (0.404 \pm 0.017(stat) \pm 0.027(sys) \pm 0.105) \times [1 - (0.031 \pm 0.004 \pm 0.003) \times p_t(\text{GeV})]$, where the last error on the normalization reflects the large uncertainty on $\mathcal{B}(\Lambda_b \to pK\pi)$.

10 Conclusions

We measure the ratio of the $\overline{B}^0_s$ yield to the sum of B^- and $\overline{B}^0$ yields as $[f_s/(f_u + f_d)]$ as $0.134 \pm 0.004^{+0.011}_{-0.010}$, and we find it to be independent of η of the $\overline{B}^0_s$ and p_t of the $D_s\mu$ system. LHCb measures this ratio also from the decay modes $B^0 \to D^-\pi^+$, $B^0 \to D^-K^+$, $B^0_s \to D^-_s\pi^+$ [23], and obtains $[f_s/(f_u+f_d)] = 0.127 \pm 0.009 \pm 0.009 \pm 0.010$, where the last error reflects theoretical uncertainties. The two results are consistent. The ratio of Λ_b yield to the sum of B^- and $\overline{B}^0$ varies with the p_t of the $\Lambda_c\mu$ pair, assuming a linear dependence, we get $[f_{\Lambda_b}/(f_u+f_d)] = (0.404 \pm 0.017 \pm 0.027 \pm 0.105) \times (1-(0.031 \pm 0.004 \pm 0.003) \times p_t(\text{GeV})$, where the multiplicative errors are statistical, experimental, and absolute scale uncertainty due to the error in $\mathcal{B}(\Lambda_c \to pK\pi)$. No η dependence is found. Furthermore, we have made the first observation of the rare semileptonic decay $\overline{B}^0_s \to D^{*+}_{s2}(2573)X\mu^-\overline{\nu}$ and measured its branching fraction relative to the total semileptonic $\overline{B}^0_s$ decay rate as $(3.3 \pm 1.0 \pm 0.4)\%$. Finally we also measured the fraction of $\overline{B}^0_s \to D^+_{s1}(2536)X\mu^-\overline{\nu}$ semileptonic decays as $(5.4 \pm 1.2 \pm 0.5)\%$

References

[1] K. Nakamura *et al.*. [Particle Data Group], J. Phys. G **37**, 075021 (2010).

[2] S. Dobbs *et al.* [The CLEO Collaboration], Phys. Rev. D **76** 112001 (2007).

[3] J. Alexander *et al.* [The CLEO Collaboration], Phys. Rev. Lett. **100**, 161804 (2008).

[4] R. Aaij *et al.* [The LHCb Collaboration], Physics Letters B **694** (2010) 209 arXiv:1009.2731 [hep-ex]. For more details see CERN-LHCb-ANA-2010-003 at http://cdsweb.cern.ch/record/1295898?ln=en .

[5] T. Sjöstrand, S. Mrenna and P. Skands, "PYTHIA 6.4: Physics and manual", JHEP **05** (2006) 026.

[6] P. d. A. Sanchez *et al.* [The BABAR Collaboration], arXiv:1012.4158 [hep-ex].

[7] M. Artuso, E. Barberio, and S. Stone, PMC Physics A (2009) 3:3.

[8] P. Urquijo, "Semileptonic B Branching Fractions," internal note (2010).

[9] A. V. Manohar, M. B. Wise, Phys. Rev. **D49**, 1310-1329 (1994). [hep-ph/9308246].

[10] I. I. Y. Bigi, M. A. Shifman, N. G. Uraltsev and A. I. Vainshtein, Phys. Rev. Lett. **71**, 496 (1993).

[11] I.I Bigi, T. Mannel, N. Uraltsev, [arXiv:1105.4574v1 [hep-ph]] (2011).
[arXiv:hep-ph/9304225].

[12] R. Aaij *et al.* [The LHCb Collaboration], Phys. Lett. B **698**, 14 (2011) [arXiv:1102.0348 [hep-ex]].

[13] V. M. Abazov *et al.* [The D0 Collaboration], Phys. Rev. Lett., **102**, (2009) 051801.

[14] D. Scora and N. Isgur, Phys. Rev. D **52**, 2783 (1995) [arXiv:hep-ph/9503486].

[15] D. Barlow, C. Beeston, Comp. Phys. Comm., **77**, 219 (1993).

[16] T Aaltonen *et al.* [The CDF Collaboration], Phys. Rev. D **79** 032001 (2009).

[17] M. Mangano, talk given at "Charm and bottom quark production at the LHC" CERN, Dec 3 2010

[18] T. Aaltonen *et al.* [The CDF Collaboration], Phys. Rev. D **77**, 072003 (2008) [arXiv:0801.4375 [hep-ex]].

[19] Private communication from M. Cacciari, P. Nason, S. Frixione, M. Mangano, and G. Ridolfi. See also M. Cacciari, S. Frixione, M. L. Mangano, P. Nason and G. Ridolfi, JHEP 0407 (2004) 33; M. Cacciari, M. Greco and P. Nason, JHEP **9805** (1998) 007.

[20] P. Sanchez *et al.* [The BABAR Collaboration], [arXiv:1012.4158 [hep-ex]] (2010).

[21] Heavy Flavor Averaging Group, http://www.slac.stanford.edu/xorg/hfag/osc/PDG_2010 (2010).

[22] M. Pervin, W. Roberts, and S. Capstick, Phys. Rev. C **72** 035201 (2005).

[23] The LHCb Collaboration, LHCb-CONF-2011-013 (2011).

Appendix A: $\overline{B}_s^0 \to D_s^+ \mu^- \overline{\nu} X$ detection efficiencies

In $\overline{B}_s^0$ semileptonic decays to charm the b changes to a c quark, and if a single hadron is formed it could be a D_s, D_s^*, or D_s^{**}. We have already discussed and measured the case where a DK combination is produced either via a D_s^{**} or fragmentation. The cases where D_s, D_s^*, and D_s^{**} (or non-resonant $D_s\pi^0$) are produced lead to somewhat different detection efficiencies, so we need to model these fractions carefully. The efficiencies are listed in Table 11.

Table 11: Monte Carlo simulated efficiencies for the different D_s final states in $\overline{B}_s^0$ semileptonic decay

Final State	Mass (MeV)	Efficiency (%)
D_s	1968	1.22±0.02
D_s^*	2112	1.17±0.02
D_{s0}^*	2317	0.99±0.02
D_{s1}	2460	0.99±0.01
D_{s1}'	2536	0.92±0.01

We ascertain the various components by using an analysis that measures the fractions by first computing the 4-momentum transfer between the $\overline{B}_s^0$ and D_s (q^2) by using the measured direction of the $\overline{B}_s^0$ candidate and momentum and energy conservation to evaluate the $\overline{B}_s^0$ momentum.

This procedure is only sufficiently accurate to determine the D_s fraction. To proceed further we take the D_s^*/D_s ratio to be the same as in B^- or $\overline{B^0}$ decays, 2.42±0.10. We first studied only the q^2 distributions and then performed the joint $q^2 - M(D_s\mu)$ fit described before. Table 12 summarizes the results and the overall efficiency obtained with different methods. By comparing the different fits, and changing the D^{**} mix, we get an overall error of 3% associated to the uncertainty in the hadron spectrum in $\overline{B}_s^0$ semileptonic decays.

Table 12: Summary of q^2 fits and efficiency for the final state $D_s\mu^-\overline{\nu}X$.

fit procedure	$f(D_s)$	$f(D_s^*)$	$f(D_s^{**})$	$\epsilon(D_s\mu)(\%)$
q^2	0.26	0.63	0.11	1.16
$q^2 - M(D_s\mu)$	0.24	0.57	0.18	1.15

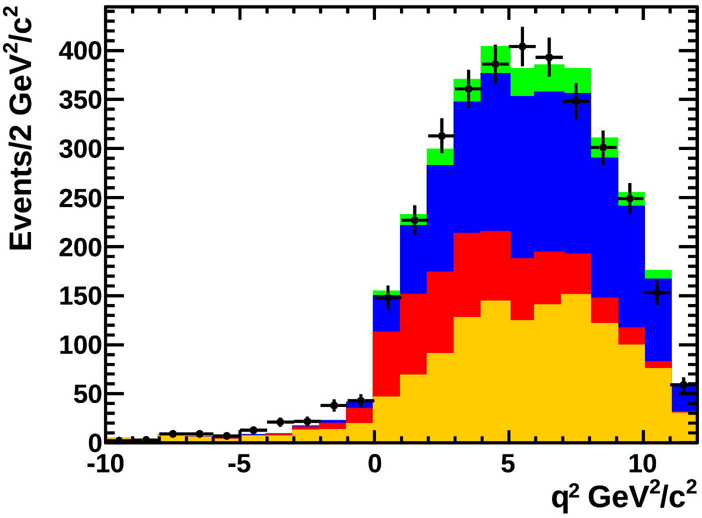

Figure 41: Fits to the q^2 distribution of semileptonic decays including a D_s meson. The D_s^*/D_s ratio has been fixed to the average value found for D^*/D in light B decays based on the similar ratio in $\overline{B}^0, B^-$ semileptonic decays (2.42±0.10), and the background contribution obtained using data fixed from the sidebands in the $K^+K^-\pi^+$ mass spectrum. The fitted decay fractions are Sideband (Orange), D_s (Red), D_s^* (Blue), and D_s^{**} (Green).

Appendix B: Study of $b \to D_s K X \mu^- \overline{\nu}$

Using $\epsilon(B^+ \to D_s^+) = (0.73 \pm 0.03\%)$ and the BaBar branching fraction for $B \to D_s K \mu^- \overline{\nu} X$ [20], we predict a yield of 35±8 $B^+ \to D_s K \mu^- \overline{\nu}$ events, corresponding to a reduction in the $\overline{B}_s^0 \to D_s X \mu\nu$ yield of 3.3%, taking into account the isospin conjugate channel $B^0 \to D_s K^0 \mu^- \overline{\nu} X$.

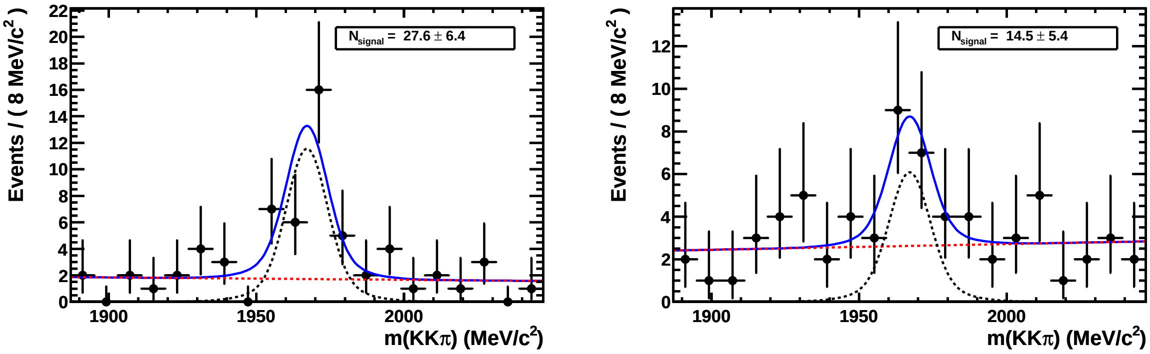

Figure 42: Invariant mass of the $K^+K^-\pi^+$ combination in the [M$(D_sK) - M(D_s)$] signal region: the left plot corresponds to the RS combinations and the right plot corresponds to the WS combination. The black dashed curve shows the signal fit.

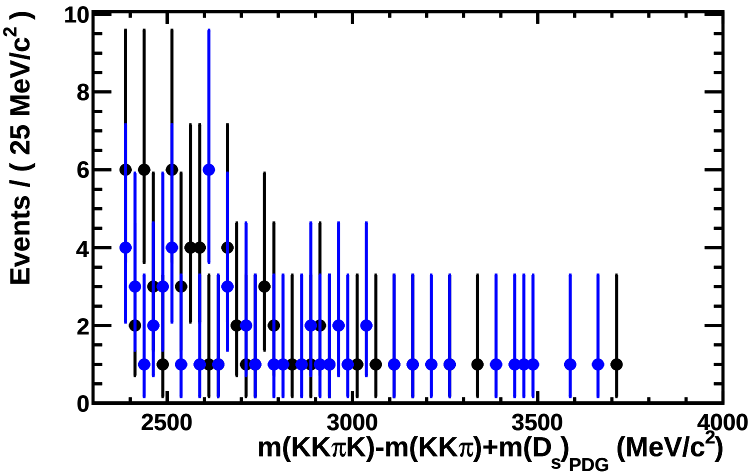

Figure 43: $D_s K \mu\nu$.[M$(D_sK) - M(D_s)$] spectrum: black points correspond to RS and blue points correspond to WS.

We also searched explicitly for $b \to D_s K \mu^- \overline{\nu}$ final states. We used the same criteria as in the $b \to D_s \mu^- \overline{\nu} X$ and $b \to D^0 K \mu^- \overline{\nu} X$final states, with the exception of the vector sum of the D_s and K transverse momenta, set to 2.17 GeV. We obtain the spectra shown in

Figs. 42 and 43. Taking the difference between the RS an WS fitted yield, we obtain 25± 11 events. We studied background components arising form cascade charm B decays, and K randomly associated with $\overline{B}_s^0 \to D_s\mu^-\overline{\nu}X$ decays using MC, and derived an estimate of 5±3 RS background events and 10±3 WS background events. Thus this approach gives 30±11 events (consistent with the previous estimate). We do not see any evidence for resonance substructure in this sample.

Appendix C: Study of $b \to D^+K^-X\mu^-\overline{\nu}$

A check suggested by the referees was a study of the final state $D^+K^-X\mu^-\overline{\nu}$. We do not expect this final state to arise in $\overline{B}_s^0$ semileptonic decays, although it could arise in $B^+ \to D^+K^-K^0X\mu^-\overline{\nu}$ semileptonic decays, where the hadronic system is produced via $d\bar{d}$ and $s\bar{s}$ popping at the lower vertex.

We apply all the selection criteria adopted in the b fraction analysis. In addition, we apply the following requirements to the additional hadron:

1. D IP > 0.05 mm,
2. DLL(K-π) > 4,
3. $p_T > 300$ MeV,
4. clone rejection (CloneDist ≤ 0),

In addition we require $p_T(D+K) > 2.17$ GeV.

Again we study the right sign and wrong sign samples. In order to determine the yields, we have used the 3 pb^{-1} sample. Fig. 44 shows the fits of the D^+ mass in the right and wrong sign samples, while Fig. 45 shows the mass difference projection. No excess is found.

We have studied possible background sources with generic b MC. The first background source considered is a random K combined with $b \to D^+\mu^-\overline{\nu}X$. This MC predicts 15.5±RS events and 25±9 WS background events in 3 pb^{-1}. In addition we have studied backgrounds coming from combinations of uncorrelated μ, D^+, and K^- combinations from b decays. This background is negligible and charge symmetric.

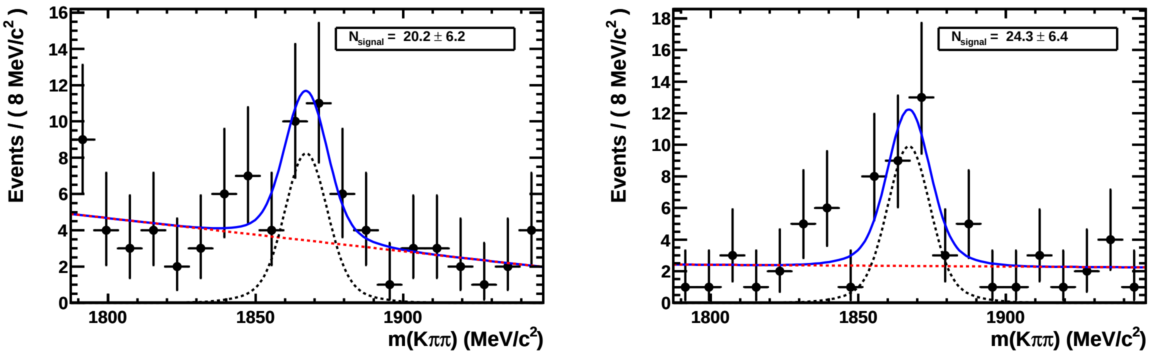

Figure 44: Invariant mass of the $K^-\pi^+\pi^+$ combination in the [M(D^+K) $- M(D^+)$] signal region: the left plot corresponds to the RS combinations and the right plot corresponds to the WS combination. The black dashed curves correspond to the signal fit.

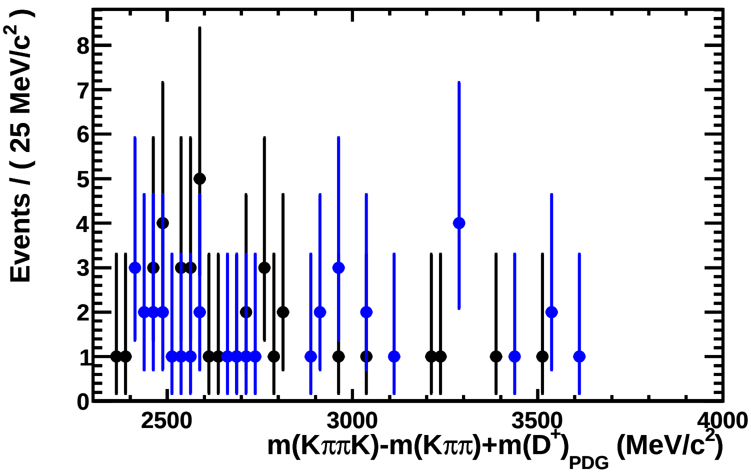

Figure 45: $D^+K\mu\nu$: RS data points black, WS data points blue.

Appendix D: $\Lambda_b \to \Lambda_c^+$ detection efficiency

In the standard LHCb Monte Carlo, Λ_b semileptonic decays are simulated using a phase space model. In order to assess the efficiency in a more realistic manner we have implemented a form factor model in EVTGEN based on the three exclusive semileptonic decays: $\Lambda_b \to \Lambda_c \mu^- \overline{\nu}$, $\Lambda_b \to \Lambda_c^\star(2595)\mu^- \overline{\nu}$, and $\Lambda_b \to \Lambda_c^\star(2625)\mu^- \overline{\nu}$. This model follows an approach similar to ISGW2 [14].

We have used this model to estimate the efficiencies in the exclusive channels shown in Table 13.

Table 13: Monte Carlo simulated efficiencies for the different $\Lambda_c^{(\star}$ final states in Λ_b semileptonic decay

Final State	Mass (MeV)	Efficiency (%)
Λ_c	1968	0.90±0.013
$\Lambda_c(2595)$	2595	0.71±0.017
$\Lambda_c(2625)$	2625	0.71±0.013

In order to derive the overall efficiency, we study the semi-exclusive channel $\Lambda_b \to \Lambda_c \mu^- \overline{\nu} X$, neglecting the X 4-vector and inferring the ν 4-momentum with the same method used for the $\overline{B}_s^0$ semileptonic studies. We use the qsq-$M(\Lambda_c - \mu)$ pdf's derived from MC for the three modes considered, plus a background pdf derived from the sideband sample. We perform a binned maximum likelihood fit to the measured q^2-$M(\Lambda_c - \mu$ distribution. As the pdfs for the two excited charmed baryon resonances are very similar, we combine them with the ratio predicted by theory (f(Λ_c(2625))/f(Λ_c(2595))=2.124. Note that the preliminary ratio between these two final states obtained from our study of the final state $\Lambda_c \pi^+ \pi^-$ is 2.9 ±0.6. Fig. 46 shows the projection of this fit along the q^2 and $m(\Lambda_c - \mu)$ axis, with the individual components. The resulting overall efficiency is 0.83±0.01 $\pm$ 0.02.

We have also studied the projections in the Dalitz plot of the invariant mass squared $m^2(\pi K)$, $m^2(p\pi)$ and $m^2(pK)$. The comparison between the 2 dimensional distributions is shown in Fig. 47. We have reweighed MC events to match the observed distributions and we derive an efficiency correction of +2.5%.

Figure 46: Two dimensional fits to the measured q^2 and $m(\Lambda_c\mu)$ distributions: the red dotted curve represent the Λ_c components, the purple and blue distribution represent the $\Lambda_c(2625)$ and $\Lambda_c(2595)$ respectively, and the black dotted curve represents the combinatoric background described by the sidebands.

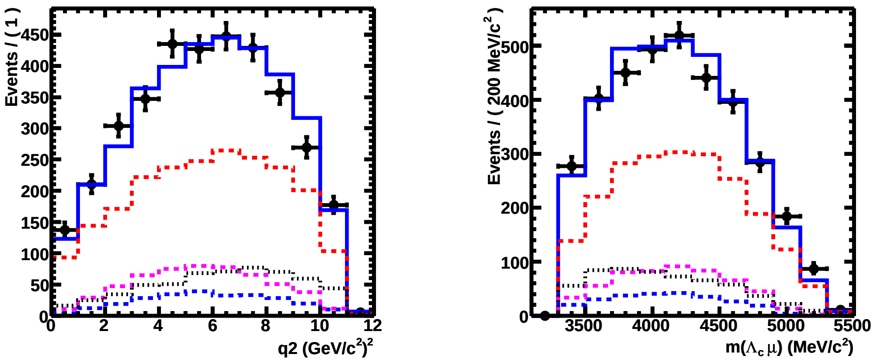

Figure 47: Comparison of Dalitz projections in data and MC for $\Lambda_c \to pK\pi$: the top represents the data (after sideband subtraction), while the bottom represents the signal MC.

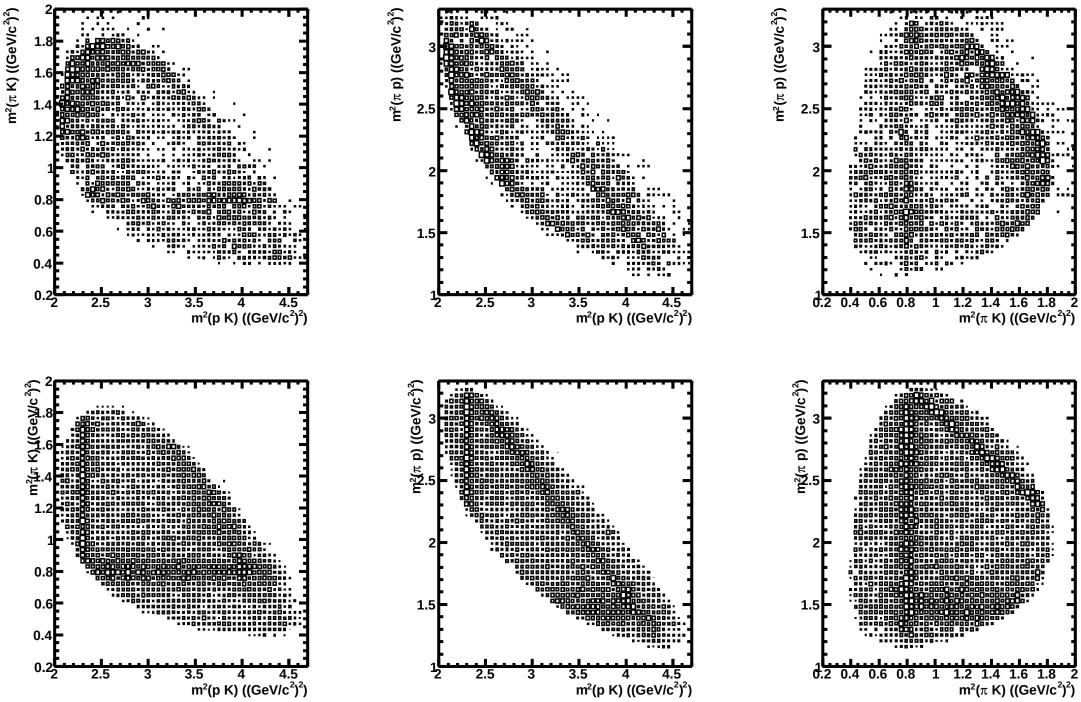

Appendix D: Studies of semileptonic decays $\Lambda_b \to \Lambda_c(2595)\mu^-\overline{\nu}X$ and $\Lambda_b \to \Lambda_c(2625)\mu^-\overline{\nu}X$

In order to validate the theoretical constrain on the ratio between the two higher masses states produced in the Λ_b semileptonic decays, we have looked for them explicitely by studying $\Lambda_c\pi^+\pi^-$ decays prodiced in association with the μ. We have optimized the π selection criteria by maximizing the $S/\sqrt{S+B}$ ratio, where S is the signal MC and B is the wrong sign background. We have used all the 2010 data set, as the low efficiency for the low momentum pions present in this decay demand high statistics.

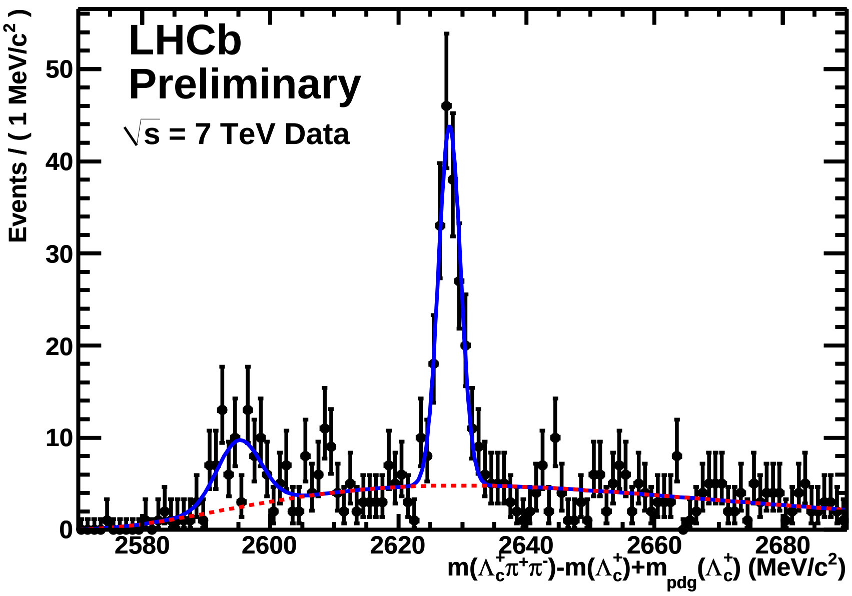

Figure 48: Measured invariant mass of the $\Lambda_c\pi^+\pi^-$ detected with a μ for $pK\pi$ invariant mass within 20 MeV of the known Λ_c mass

Table 14: Yields and efficiencies for the two final states $\Lambda_c(2625)\mu^-\overline{\nu}X$ and $\Lambda_c(2595)\mu^-\overline{\nu}X$.

	Yield	$\epsilon(\%)$
$\Lambda_c(2625)$	169±15	0.057±0.003
$\Lambda_c(2595)$	63± 12	0.063±0.003

Fig. 48 shows the mass difference plot for the RS and WS combinations. Two clear peaks can be seen at masses corresponding to the $\Lambda_c(2595)$ and $\Lambda_c(2625)$. Table 14 summarizes the yields, obtained with Gaussian fits, and the efficiencies for the two final states. While this fit will be refined in a future dedicated analysis, the preliminary value of the ratio extracted from it (2.9±0.6), where the error is only statistical, allows to assign a systematic error to the uncertainty of the Λ_b efficiency due to the uncertainty in the final state composition.

Appendix E: On the equality of b-hadron semileptonic widths

The following correspondence confirms that the semileptonics widths are equal to the 1% level.

Initial inquiry: Hi It is well known that the semileptonic width is equal for Bo and B+ mesons as it is for D0 to D+ meson. The Ds is somewhat smaller. Are there any theoretical expectations for the Bs? We need this to measure the Bs fractions at LHCb, which is important for Bs →mu+mu-, for example.
sincerely Sheldon

Response from Uli Nierste Dear Sheldon, the semileptonic width of B0 and Bs meson are expected to agree within 0.5%.

There are papers discussing the full width of Bs and Bd. In my response to your email I have adapted these results to the semileptonic width: Essentially the estimates in Eqs. (55) and (56) of the paper by Beneke, Buchalla and Dunietz, Phys.Rev.D54:4419-4431,1996 (hep-ph/9605259) for the total width apply to the semileptonic widths as well. (The other discussed contribution, "WA", is absent for the semileptonic width.) An update of the ratio of the total Bd, Bs widths is in Phys.Rev.D57:4282-4289,1998 (hep-ph/9710512), a paper by Keum and me.

But there are earlier papers which pointed out that the semilptonic widths of Bd and Bs mesons are essentially equal, I remember Ikaros Bigi writing this often. But I do not have a reference at hand.
Best regards, Uli

Response from Gerhard Buchalla Hi Sheldon,

my short answers is: I expect the semileptonic width of the Bs to be the same as the one of B0, to within less than 1%.

More precisely, the heavy-quark expansion for the semileptonic width of a B-meson gives

$Gamma_l(B) = GF^2 mb^5/(192pi^3)|Vcb|^2[z3(1 + (lambda1 + 3lambda2)/2/mb^2) + z56lambda2/mb^2]$

(neglecting b-→u transitions). z3 and z5 are (quark-level) phase-space factors. The by far dominant contribution comes from free b-quark decay and is universal to B0, B+ and

Bs. A difference between these cases can arise from the hadronic quantities lambda1 and lambda2, which enter at second order in 1/mb. The effect of the second order corrections is 2-3 %. The difference between B0 and Bs then can come from SU(3) breaking in these small corrections, which is about 10% for lambda2. lambda1 is more uncertain but its impact is only about 1%. The semileptonic widths of B0 and Bs should then be equal to within several permille.

The Ds vs. D0 semileptonic width difference can easily be larger because of the much larger power corrections for charm.

Best regards,

Gerhard

Response from Dimitri Melnikov

Dear Sheldon, I've made a simple calculation similar to Ligeti et al PRD82, 033003 (2010) [details in the attached mathematica file] and obtained in the SU(3)limit and up to $1/mb^4$ corrections:

$Gamma_S L(Bd) - Gamma_S L(Bs) = 0$

$Gamma_S L(Bu) - Gamma_S L(Bs) = O(Vub^2)$.

So, all three SL rates should be equal to each other.

Best regards, Dmitri

Response from Michael Gronau

Hi Sheldon;

Indeed, while the semileptonic width is equal within errors for D0 and D+ it is somewhat smaller for Ds. Taking an average for the widths of D0 and D+, this difference (of order 15%) is a 3.2 sigma effect.

This difference is expected to be much smaller in the B system as it behaves like $1/m_q^2$ where q=c for D and q = b for B. I think you may safely assume that the difference between the leptonic width for B0 or B+ and for Bs should be smaller than one percent.

I am cc-ing this note to Jon Rosner who may have some comments.

Regards, Michael

Response from Jon Rosner

For the ratio of Ds l nu to D l nu rates I got 1.0140 while for the ratio Ds* l nu to D* l nu rates I got 1.0081. Taking the spin-weighted average, I got almost exactly a 1% enhancement of the Bs SL rate relative to the B SL rate.

Now I am curious to see if the 1/mb expansion calculations get anything like this. I can also do the same calculation for D and Ds semileptonic decays, but the problem in the Ds case is that the pseudocalar s sbar strength is distributed among eta and eta'.

Regards, Jon

Response from Michael Gronau to Rosner

Checking your calculation I obtain slightly larger values, 1.01618 instead of 1.0140 and 1.00974 instead of 1.0081. I used the following ratios of squared masses, $r = m_D^2/m_B^2$ etc: r = 0.125404, $r_s = 0.134557$; r* = 0.144982, $r*_s = 0.154939$.

The spin-averaged value is, indeed, almost exactly a 1enhancement of Bs SL rate relative to the B SL rate. I obtain an averaged ratio of 1.011. (I think your averaged value is 1.010).

Regards, Michael

Calculation of Semileptonic D decay widths from Rosner

I have to re-check, but the same calculation for D vs. Ds gives a ratio of $R = Gamma_{SL}(Ds)/Gamma_{SL}(D)$ depending on the relative s sbar strengths in eta and eta':

Eta Eta' Ratio Comments fraction fraction R

1/3 2/3 0.814 Frequently used mixing

1/2 1/2 0.886 "Isgur" mixing

Most phenomenological fits to processes involving eta and eta' fall between these two extremets. Pure octet eta and pure singlet eta' correspond to 2/3 and 1/3, respectively.

Experimentally I find R = 0.830 +- 0.053 based on PDG 2010 values.

So the calculation does not give crazy results for charm.

Of course one should be able to test it by comparing predictions for actual semileptonic widths, but I suspect there might be some tradeoff between vector and pseudoscalar widths when using the naive fermionic formula. Maybe the ratio of Ds =¿ eta' l nu to Ds =¿ eta l nu rates would be more relevant. I intend to consult:

Studies of $D^+ \to \{\eta', \eta, \phi\} e^+ \nu_e$, J. Yelton *et al.* [CLEO Collaboration], clns 10/2067, CLEO 10-04, arXiv:1011.1195 [hep-ex], submitted to Phys. Rev. Letters.

Regards, Jon –